A Study of Background for Detecting Appearance Signal of Neutrino Oscillation $\nu_\mu \to \nu_e$ Using a Very Long Baseline Wideband Neutrino Beam and a Large Underground Water Cherenkov Detector

C. Yanagisawa*, C. K. Jung, P. T. Le

Stony Brook University, Department of Physics and Astronomy, Stony Brook, NY 11794-3800, U.S.A.

B. Viren

Brookhaven National Laboratory, Department of Physics, Upton, NY 11973, U.S.A.

(Dated: July 18, 2006)

Abstract

In this report we describe in some detail a promising method to study ν_e appearance signal in $\nu_\mu \to \nu_e$ oscillation using a very long baseline neutrino beam directed at a very large water Cherenkov detector (0.5 Mton fiducial volume) such as UNO. This method promises to make such a long baseline neutrino oscillation experiment realistic as it strongly suppresses the initially large background coming from π^0 production by neutral current interactions while retaining good signal efficiency.

* email: chiaki@nngroup.physics.sunysb.edu

I. INTRODUCTION

It has been shown that there are certain advantages in a wideband neutrino beam over a now traditional narrowband neutrino beam for neutrino oscillation experiments provided the baseline is reasonably long (over 1,000 km) [1]. The first advantage is that a wideband beam covers more than one node (peak) in the disappearance (appearance) neutrino oscillation probability. Unlike a narrowband or off-axis beam this both reduces the dependence on the exact value of Δm^2_{31} and allows for the oscillation signature to be resolved. The second is that it places part of the $\nu_\mu \rightarrow \nu_e$ appearance signal at a high enough energy to naturally avoid the most of the primary background (π^0 from neutral current interactions).

In the original paper by the Brookhaven National Laboratory (BNL) neutrino working group (NWG) the results were based on 4-vector level Monte Carlo (MC) simulation and known resolutions but not by simulating detailed detector response of a water Cherenkov detector. In addition it was assumed that the signal events were only from quasi-elastic scattering ($\nu_e + n \rightarrow e^- + p$) and the background events were from single π^0 producing neutral current (NC) interactions ($\nu_e + N \rightarrow \nu_e + \pi^0 + N'$).

In order to gain a better insight in this idea of a very long baseline neutrino oscillation experiment, we performed a more elaborate Monte Carlo simulation that includes all known neutrino interactions, a detailed water Cherenkov detector response, and well-tuned event reconstruction algorithms. This Monte Carlo simulation together, with event reconstruction programs, was developed and fine-tuned for the Super-Kamiokande-I (SK-I) experiment [2].

In this report we define the reconstructed neutrino energy (E_{rec}) as:

$$E_{rec} = m_N E_e / [m_N - (1 - cos\theta_e) E_e]$$

Here m_N, E_e and θ_e are the nucleon mass, reconstructed recoil electron energy and the reconstructed scattering angle of the recoil electron with respect to the incident neutrino beam, respectively. This quantity best represents the true incident neutrino energy when the event is produced by charged current quasi-elastic scattering (QE) and the Fermi motion of target nucleons is small compared to the neutrino energy. The true and reconstructed neutrino energy spectra are shown in Fig. 1 for QE ν_e events.

Because ν_e QE events give the best resolution for reconstructed neutrino energy criteria are defined which predominantly select them as signal for $\nu_\mu \rightarrow \nu_e$ appearance. The signature

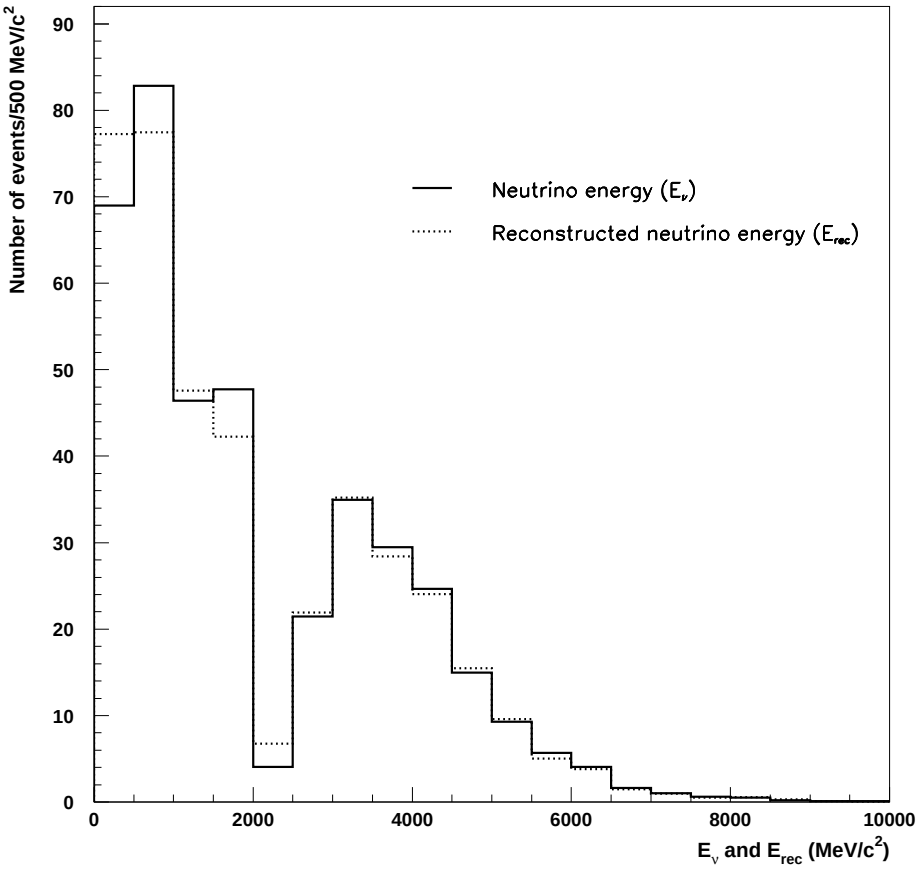

FIG. 1: The neutrino energy and reconstructed neutrino energy distribution of single electron-like ring events originating from QE.

is an event with a single electron-like (e-like) Cherenkov ring. In a water Cherenkov detector, due to the high momentum threshold for Cherenkov radiation of a proton (about 1 GeV/c), the recoil proton is invisible in most events. Above a neutrino energy of about 1 GeV, QE events are less dominant compared to inelastic-scattering processes. Some of these interactions, such as $\nu_e + N \rightarrow e^- + \pi^\pm + N'$, may also produce single e-like ring events as the momentum of the $\pi^\pm$ is often below the Cherenkov threshold of 160 MeV/c. While not as useful as pure QE events, these CC events still contain information on $\nu_\mu \rightarrow \nu_e$ oscillation and provide adequate resolution on neutrino energy.

There are three main sources of background to $\nu_\mu \rightarrow \nu_e$ appearance. The most troublesome are interactions that produce a π^0 which has only one of its decay γs found. This occurs

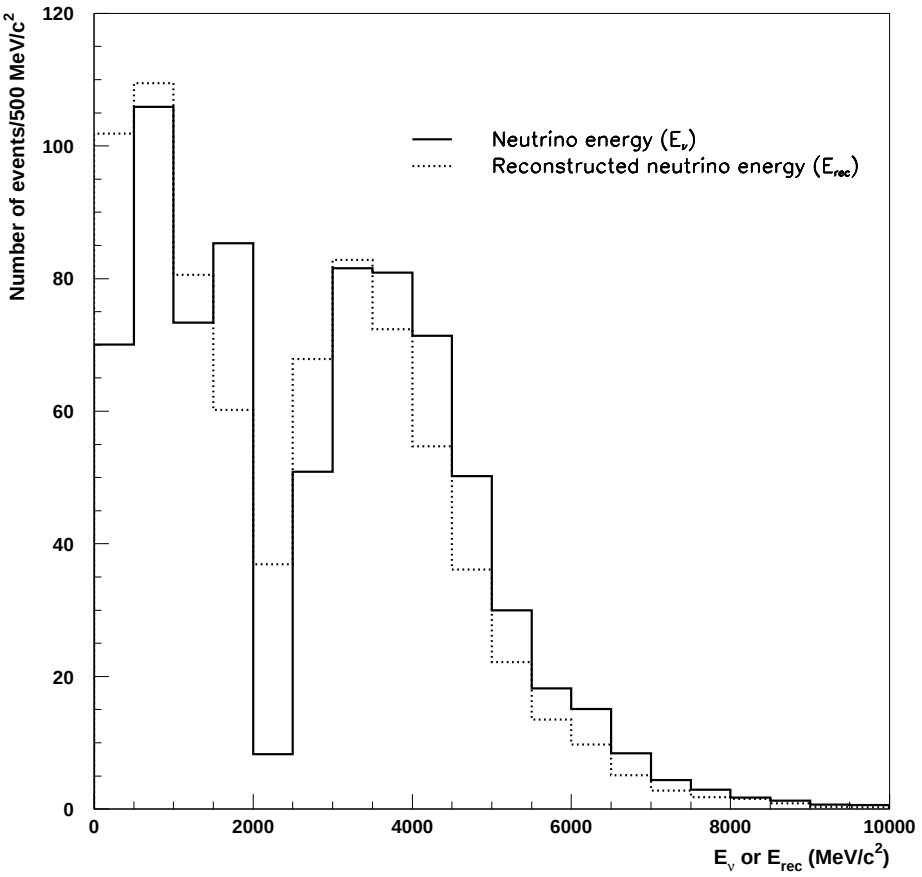

FIG. 2: The neutrino energy and reconstructed neutrino energy distribution of single electron-like ring events originating from all the charged current interactions.

in single π^0 NC events or any interactions where all other products but the π^0 are below the Cherenkov threshold. The next is the largely irreducible background due to interactions of ν_e produced in the beam (through muon or kaon decays). This intrinsic ν_e contamination is about 0.7% of, and has a similar shape as, the primary and unoscillated ν_μ component. Finally at the lowest energies, ν_μ QE events producing a μ close to Cherenkov threshold can be reconstructed as an e-like ring.

To improve the π^0 background rejection a special π^0 finder called *POLfit* [4] has been developed for SK-I. The reconstruction that precedes *POLfit* can often reconstruct a π^0 as a single e-like ring in two cases. First, when the π^0 decays asymmetrically with respect to its direction of boost in the lab frame one γ will receive the bulk of the energy and produce a

predominant ring while the second will produce a very faint or invisible one. Second, if the decay is very symmetric and the π^0 strongly boosted the two γ-rings will largely overlap.

This algorithm has to date not been used for any physics analysis published using the SK-I data because the standard reconstruction techniques separate ν_e from π^0 events at the level required. On the other hand, in the case of a neutrino beam experiment it was found to be extremely useful [5] for removing the undesirable single π^0 background events from otherwise apparently single e-like ring events. *POLfit*, together with other useful variables has been effectively used to reduce the background significantly while retaining a good efficiency for the signal.

II. MONTE CARLO EVENT SAMPLE

The Monte Carlo event sample used in this work was originally produced by the SK-I collaboration to simulate atmospheric neutrino events detected by the SK-I detector and corresponds to about 100 years of the exposure time. The detailed description of the Monte Carlo generation as well as the event reconstruction was recently published [3]. The neutrino (and anti-neutrino) spectra for ν_μ and ν_e produced in the Earth's atmosphere are quite different from those of ν_μ and ν_e produced in the neutrino beam calculated by the BNL NWG. Each reconstructed atmospheric neutrino event was given a weight such that the weighted flux spectra would agree with those of the BNL NWG beam.

The total number of weighted charged current quasi-elastic neutrino interactions is normalized to 12,000 events produced in the fiducial volume. This figure roughly corresponds to the number of ν_μ charged current quasi-elastic events expected in the absence of neutrino oscillation in the proposed long baseline experiment with a fiducial volume of 0.5 Mtons. The pertinent parameters of the experiment are:

- 500 kton fiducial mass water Cherenkov detector with SK-I like efficiencies,
- 2,540 km baseline,
- 1 MW, 28 GeV proton beam and
- operating for 5×10^7 seconds.

Details of this long baseline proposal are in the paper by the BNL NWG [1]. Since we use the Monte Carlo event sample generated for the SK-I detector, this normalization corresponds to the event rate seen by 22.2 SK-I detectors in the fiducial volume.

In the following, all the Monte Carlo events to be used are selected with this initial set of cuts:

1. exactly one e-like ring from standard reconstruction
2. reconstructed vertex is > 2 meter from the plane of photomultipliers (PMT)
3. no activity in the outer (veto) detector

Furthermore, events with reconstructed energies greater than 10 GeV are ignored due to lack of MC statistics. For the neutrino beam studied here, the background contribution from neutrino energies above 10 GeV is small.

In this report we use the following neutrino oscillation parameters: $\Delta m^2_{21} = 7.3\times10^{-5}eV^2$, $\Delta m^2_{31} = 2.5 \times 10^{-3}eV^2$, $\sin^2 2\theta_{12} = 0.86$, $\sin^2 2\theta_{23} = 1.0$, $\sin^2 2\theta_{13} = 0.04$, and $\delta_{CP} = 0^o, \pm 45^o, \pm 135^o$. Note that the sign convention of δ_{CP} follows that of the paper by BNL NWG [1]. Unless otherwise stated, in this paper the value of δ_{CP} is $+45^o$ and the baseline is 2,540 km which corresponds to the distance from BNL to the Homestake Mine in South Dakota. In later sections, we will report the results with different values for δ_{CP} as well as with the baseline of 1,480 km which corresponds to the distance from Fermilab to the Henderson Mine in Colorado.

III. POLFIT

In this section we describe briefly the π^0 reconstruction algorithm called "Pattern Of Light fit" (*POLfit*) [4]. *POLfit* works by calculating the expected charge in each PMT created by the incident Chereknov light from the showers induced by the γ decay products of a π^0. A distribution of PMT readout is for each γ as a function of its energy and direction. The sum of these two distributions is compared to the actual distribution of PMT readout and a likelihood is formed. The parameter space is then searched to maximize the likelihood with the constraint that the parameters of the dominant ring are those as found by the prior, standard reconstruction. The likelihood maximization is optimized by employing a set of

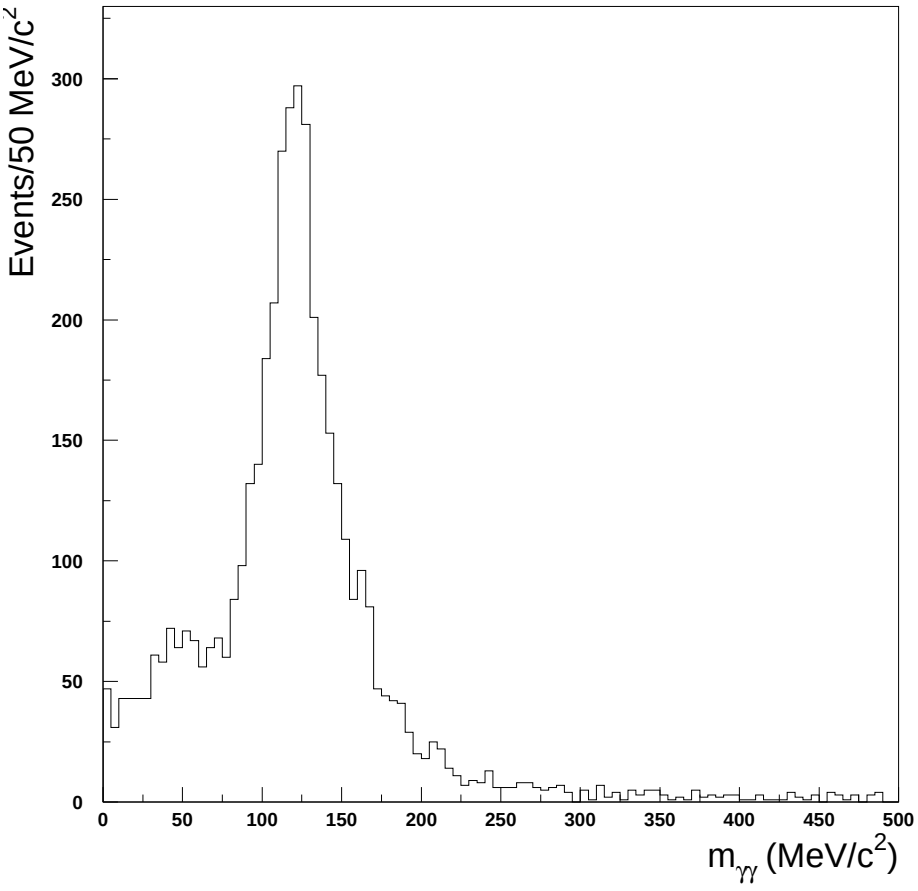

FIG. 3: Reconstructed π^0 mass of single e-like ring events from neutral current single π^0 production using *POLfit*.

predetermined *templates* each of which is a lookup table that gives distributions of PMT readout given kinematic parameters for a γ particle.

POLfit is optimized in two regions of parameter space and returns one likelihood for the case where the angle between γ directions is confined to be small (forward-algorithm) and another where the angle is not confined (wide-algorithm). In this report we use the wide-algorithm result unless otherwise stated. For all events, *POLfit* will return parameters for a fit of a secondary γ whether the event truly has two rings or not. The final result for each algorithm is an estimate for the directions and energies of the two γs, as well as the maximum likelihood and two-photon invariant mass.

To demonstrate the power of *POLfit*, first we show in Fig. 3 the two-photon invariant mass

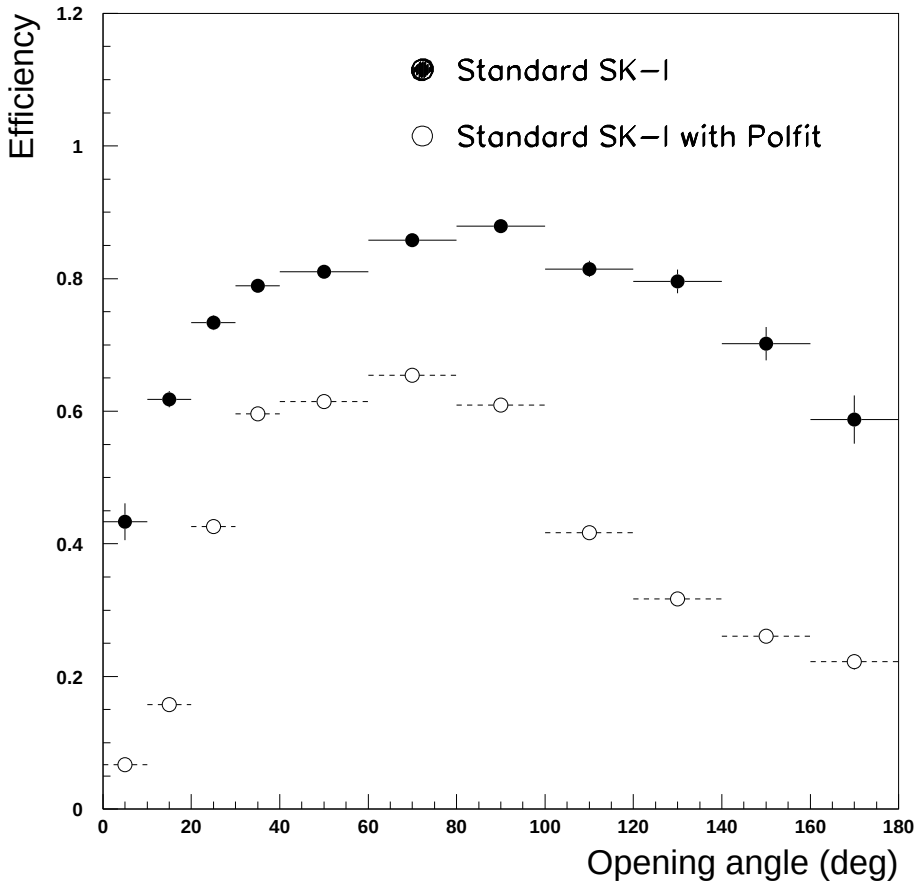

FIG. 4: π^0 reconstruction efficiency with (1- and 2-ring events, solid circles) and without (2-ring events only,open circles) *POLfit*.

distribution of single π^0 NC events reconstructed as single e-like events by the standard SK-I reconstruction software. A peak around the π^0 mass is clearly seen in the figure indicating that in most of the events *POLfit* finds the missing second photon from π^0 decay. Events off the mass peak are due to *POLfit* falling into false maxima due to the second ring being too faint or indistinguishable from the primary ring.

In Fig. 4 we also show the relative single π^0 NC reconstruction efficiencies first using the standard SK-I reconstruction and additionally applying *POLfit*. They are shown as a function of the opening angle between the two photons. In the first case, only events with two e-like rings found by the standard SK-I software are used. In the second, events where the SK-I software found either one or two e-like rings are used. Solid (open) circles represent

the efficiency with (without) *POLfit* as a function of the true opening angle between two photons. Events going into these efficiencies were selected to have a two-photon invariant mass within 2 σ around the peak correspond to the π^0 mass shown in Fig.3. Because of this cut the efficiencies are relative ones.

The reduction of π^0 detection efficiencies at the smallest opening angle is due to overlap between two e-like rings. At the largest it is due to a faint, low energy second e-like ring that is missed and goes in the opposite direction to that of the primary ring. In the first case, the two overlapping rings can be falsely reconstructed as a single ring, while in the second case the weak ring is not reconstructed. As clearly seen in Fig. 4, *POLfit* improves the π^0 reconstruction efficiency significantly.

For Figs. 3-4, the neutrino energy spectrum is that of the original, unweighted SK-I atmospheric muon neutrinos.

IV. QUANTITIES USED TO DISTINGUISH THE SIGNAL FROM THE BACKGROUND

A simple cut on $m_{\gamma\gamma}$ is effective but cannot be solely used to reduce the background to ν_e appearance. It will cut into the signal quickly as one increases the amount of background rejected. Additional quantities that distinguish the signal from the background in single e-like ring events must be developed. In this section we describe nine such quantities including $m_{\gamma\gamma}$. While none alone can decisively separate signal and background, each contributes some selective power. All the distributions in this section are plotted for the different E_{rec} regions in steps of 0.5 GeV from 0 to 2 GeV, 2 GeV$\leq E_{rec} <$ 3 GeV, and 3 GeV$\leq E_{rec}$.

A. Reconstructed π^0 mass $m_{\gamma\gamma}$ ($m_{\gamma\gamma}$)

This quantity is quite useful to remove some unwanted background events from single π^0 production. In Fig. 5 the distributions of this quantity in different reconstructed neutrino energy regions for signal events (solid line) and for background events (dotted line) are plotted. In the lower reconstructed neutrino energy region ($E_{rec} \leq 2$ GeV), the distribution shows a prominent π^0 peak. As the energy goes higher, contributions from multi-pion production increase and *POLfit* often either fails to find the right photon or badly reconstructs

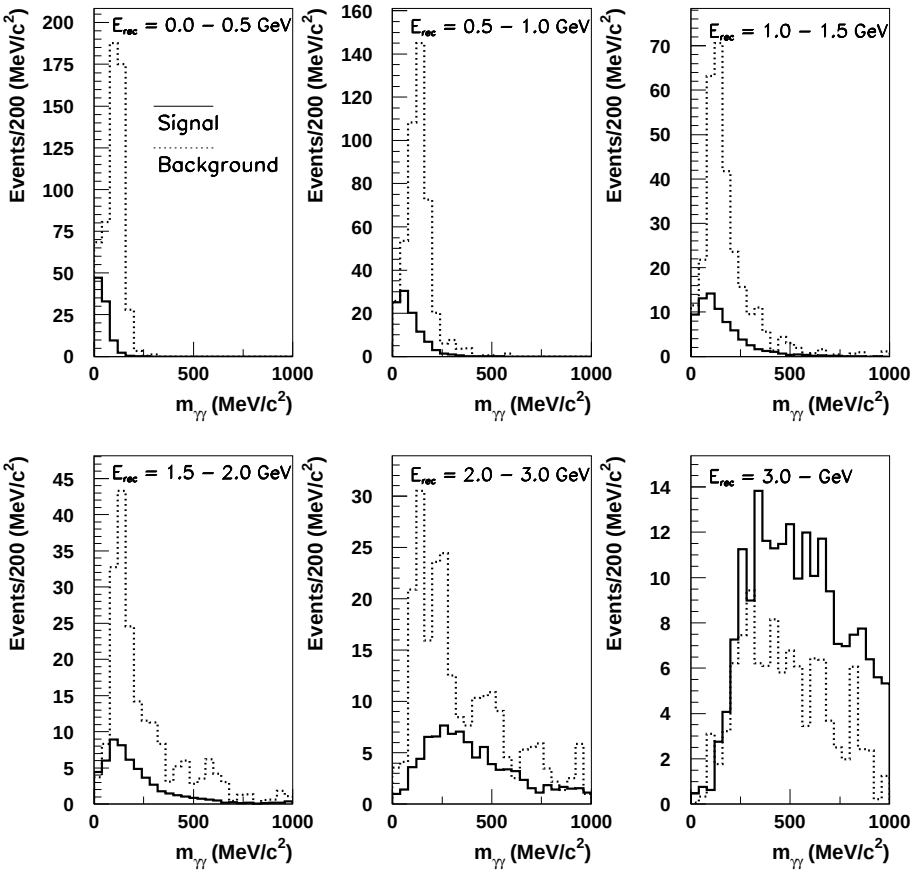

FIG. 5: Distributions of reconstructed π^0 mass of single e-like ring events for signal (solid line) and background (dotted line).

the correct photon ring. This is the reason that the π^0 peak disappears in the higher energy region.

B. Fraction of energy in the second ring ($\mathbf{E}_{frac}$)

In general, the second ring found by *POLfit* has smaller energy than the primary e-like ring found by the standard SK-I reconstruction software. Furthermore a fake ring falsely reconstructed by *POLfit* tends to have much less energy than the primary ring. This is seen in Fig. 6 where the ratio of the energy of the second ring to the sum of both ring energies is shown. The difference between the signal and background distributions is less pronounced

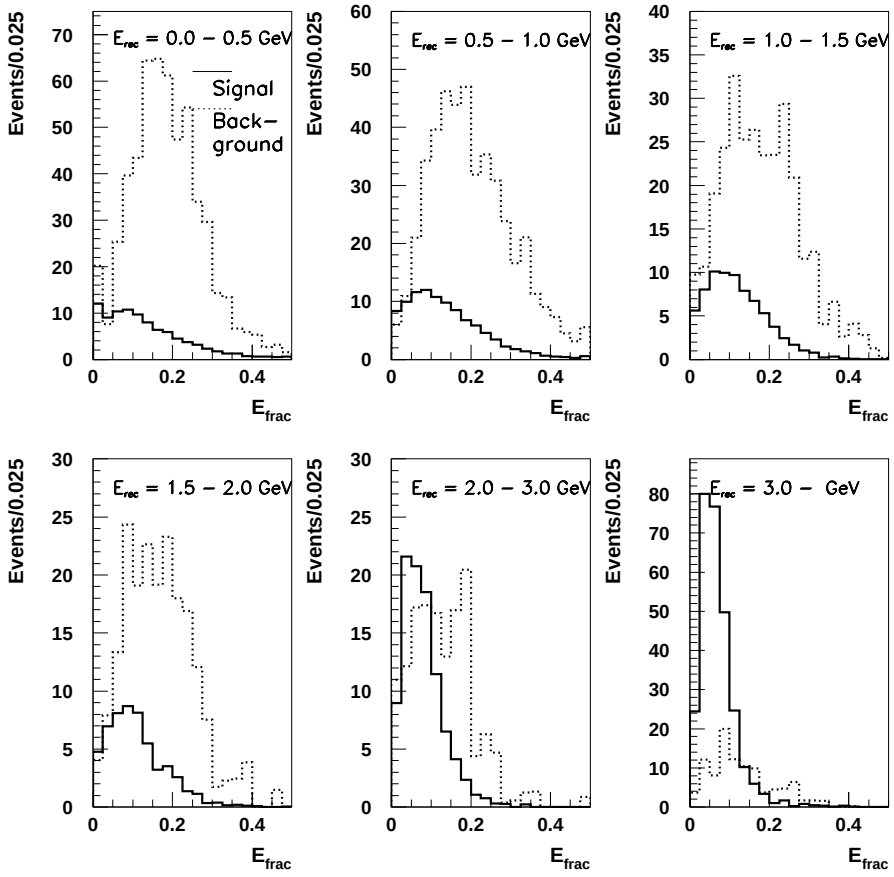

FIG. 6: E_{frac}: The distributions of the energy fraction of the second ring found by *POLfit* in 1-ring events for the signal (solid line) and background (dotted line).

but still exists in the higher energy region.

C. Difference in log π^0 likelihood ratio ($\Delta \log \pi^0$-lh)

As mentioned above, *POLfit* deploys two algorithms: the wide- and forward-algorithm. Each algorithm provides a log-likelihood that the detector response is due to a π^0. For events containing a single electron, both algorithms tend to place the falsely reconstructed second (fake) ring in the vicinity of the primary ring. On the other hand, when the event is actually due to a π^0 decay, the two algorithms will give differing log-likelihood values. This difference in the log-likelihood is pronounced in lower energy region as shown in Fig. 7. However, this

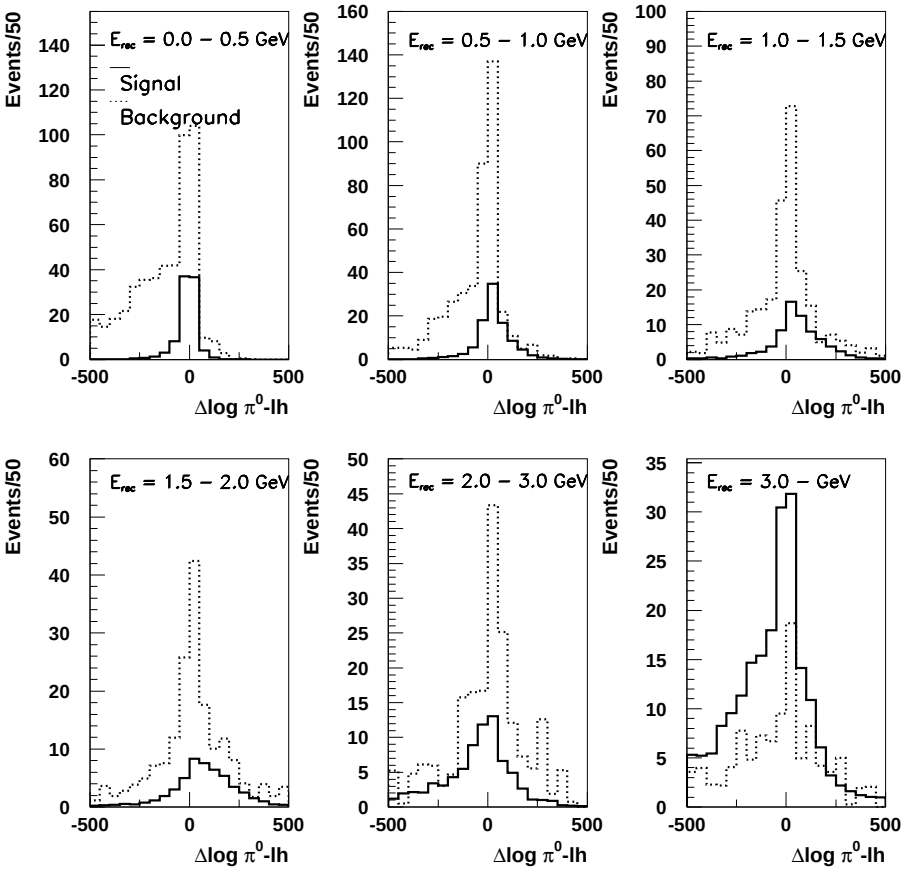

FIG. 7: $\Delta \log \pi^0$-lh: The distributions of the difference in log π^0 likelihood between the two algorithms. The larger this quantity, the more likely an event is π^0 background. The distribution in solid line is for the signal and that in dotted line is for the background.

trend changes above $E_{rec} = 1.0$ GeV where the contribution from deep-inelastic scattering starts to increase.

D. Direction cosine of the e-like ring ($\cos\theta$)

The direction cosine of the primary e-like ring, found by the standard reconstruction, with respect to the neutrino beam is a good discriminator to separate the signal from the background. This quantity does not depend on the information from *POLfit*. When E_{rec} is below 1.5 GeV/c^2, the major background source comes from single π^0 neutral current

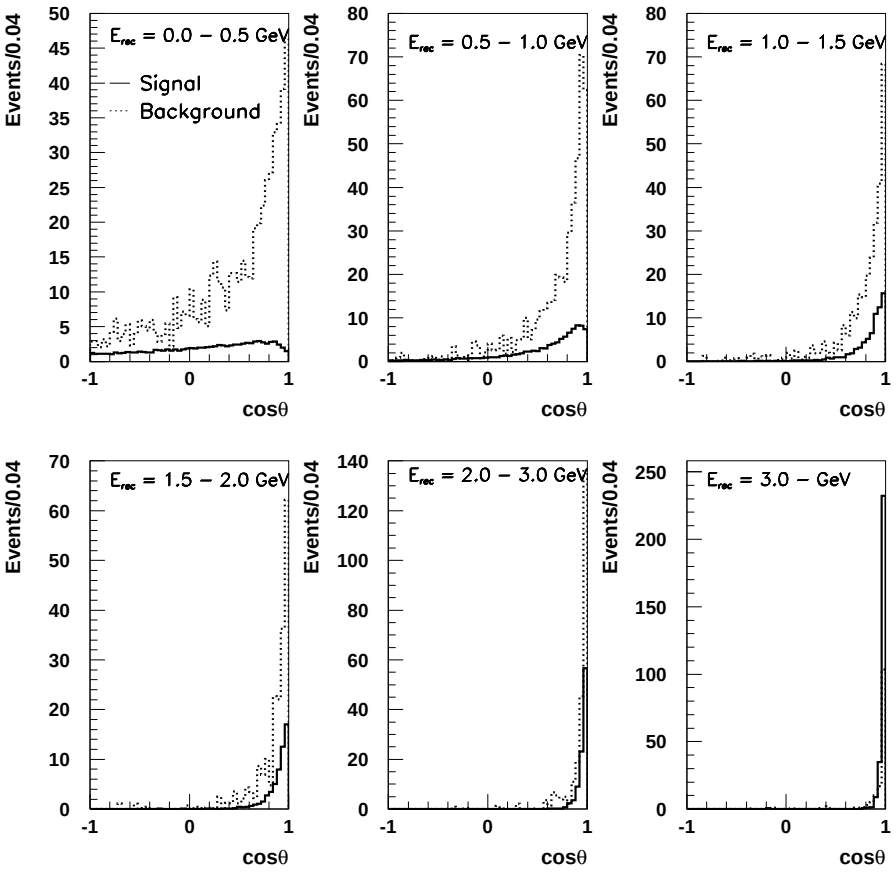

FIG. 8: $\cos\theta$: The distributions of the directional cosine of the primary e-like ring with respect to the neutrino beam direction. The distribution in solid is for the signal and that in dotted is for the background.

events, while the signal events are mainly from QE events. Due to the Fermi motion of the target nucleon, the recoil electron in a signal event is scattered more than the π^0 from a background event in the lower neutrino energy region. Since we require that a candidate signal event contain a single e-like ring, the second lower-energy photon from a π^0 decay event is missed and the majority of the π^0 energy is carried visible as the primary e-like ring. This is another reason why the electron in a signal event is scattered more than the primary photon in a background event, as clearly seen in Fig. 8.

E. Ratio: Total charge to ring energy (Q/E)

If an event contains an unreconstructed second ring, it will have extra light detected by PMTs beyond that attributed to the single primary ring that is reconstructed by the standard SK-I software. Because of this the ratio of the total charge recorded by PMTs in unit of photoelectron (pe) to the reconstructed energy of the primary ring in MeV is expected to be distributed differently for the signal than for the background events. The background events have more total charge than what can be attributed to a single ring as it has an extra energy deposit from the second missed ring. Fig. 9 shows the distribution of this ratio. As expected, the distribution for the background events has more events in higher values than that for signal events.

F. Difference in log pid-likelihood (Δlog pid-lh)

The standard SK-I reconstruction software provides likelihoods of a Cherenkov ring to be e-like (L_e) and to be muon like or μ-like (L_μ). From these two particle identification likelihoods (pid-likelihoods), the difference between two log pid-likelihoods, $\log(L_\mu/L_e)$ (Δlog pid-likelihood) is used as a good measure to separate electrons from muons. The more negative log pid-likelihood is, the more e-like a Cherenkov ring is. This quantity can also be used to separate π^0 and single electron events. Even though the two photons are reconstructed as a single e-like ring they may not fully overlap. This causes a broader and fuzzier pattern of Cherenkov light and thus a more negative log pid-likelihood. As the reconstructed energy increases and the rings overlap more this becomes a weaker discriminant. Fig. 10 shows this behavior of log pid-likelihood as a function of E_{rec}.

G. $\log \pi^0$-likelihood ($\log \pi^0$-lh)

POLfit provides the logarithm of a likelihood that the event is due to a single π^0. For events that truly come from a single π^0 this quantity is expected to be smaller (more negative) than that for single electron signal events. This trend shows up in lower energy region ($E_{rec} \leq 1$ GeV) as shown in Fig. 11. In higher energy region, the distribution tends to be narrower for the signal events.

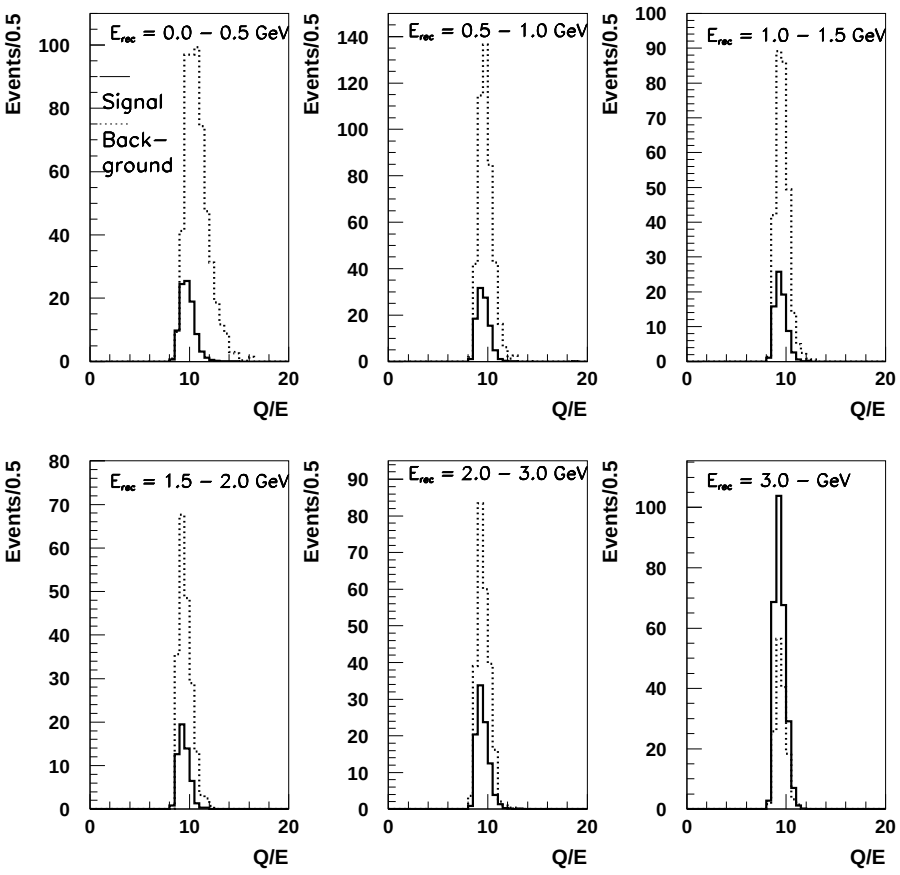

FIG. 9: Q/E: the distributions of the ratio of the total charge in pe to the ring energy in MeV are shown. The distribution in solid is for the signal and that in dotted line is for the background.

H. Cherenkov angle (Cangle)

The distribution of the reconstructed Cherenkov angle is expected to be different between the signal and background events and also depends on whether there is overlap between two Cherenkov rings and on the energy of the primary ring. In Fig. 12 the Cherenkov angle distributions for the different E_{rec} regions are shown. The shape of the distribution for the signal events differs from that for the background events in most of energy regions, although degrees of differences vary from energy region to region.

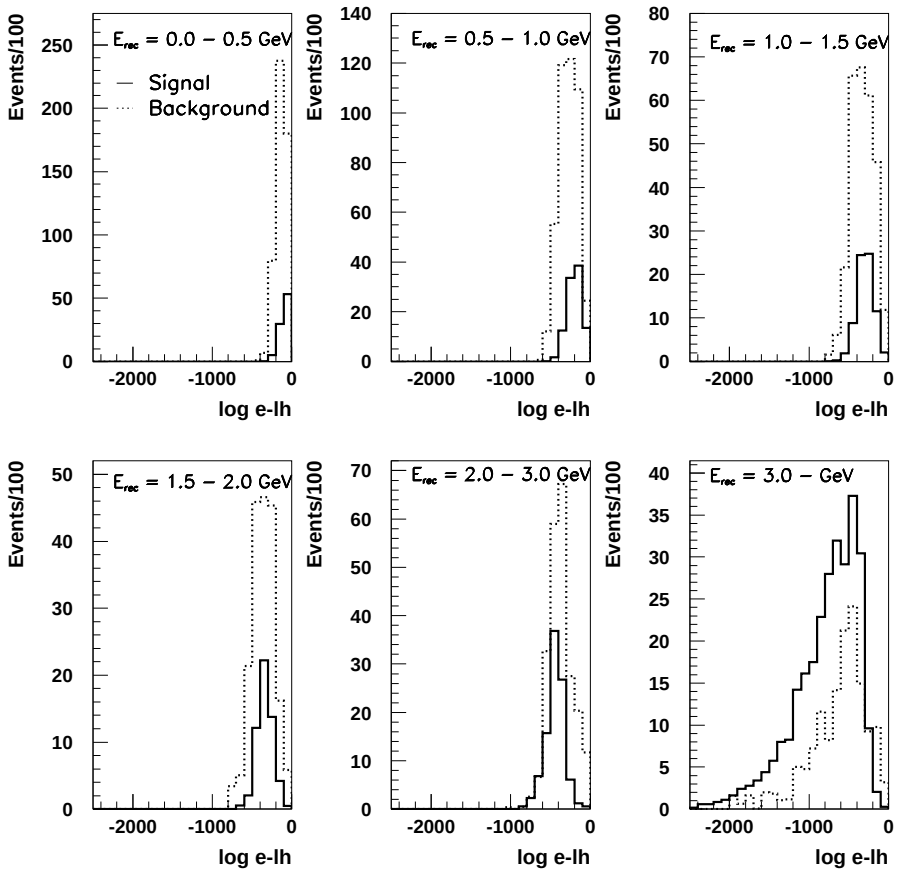

FIG. 10: Δlog pid-lh: The distributions of the difference in log pid-likelihood between e-like and μ-like of the primary e-like ring. The solid line stands for the signal and the dotted line is for the background.

I. Difference in log ring-count likelihood (Δ log ring-lh)

To decide how many Cherenkov rings there are in an event, two hypotheses are compared. The first hypothesis is that there is only one Cherenkov ring. The second is that there is an additional ring in the event. The comparison is made using difference in log likelihood (log-likelihood) of the two hypotheses. In Fig. 13, this difference in log-likelihood is plotted for the different E_{rec} regions. The shape of the distribution for the signal events differs from that for the background events in most of the energy regions with varying degree of differences.

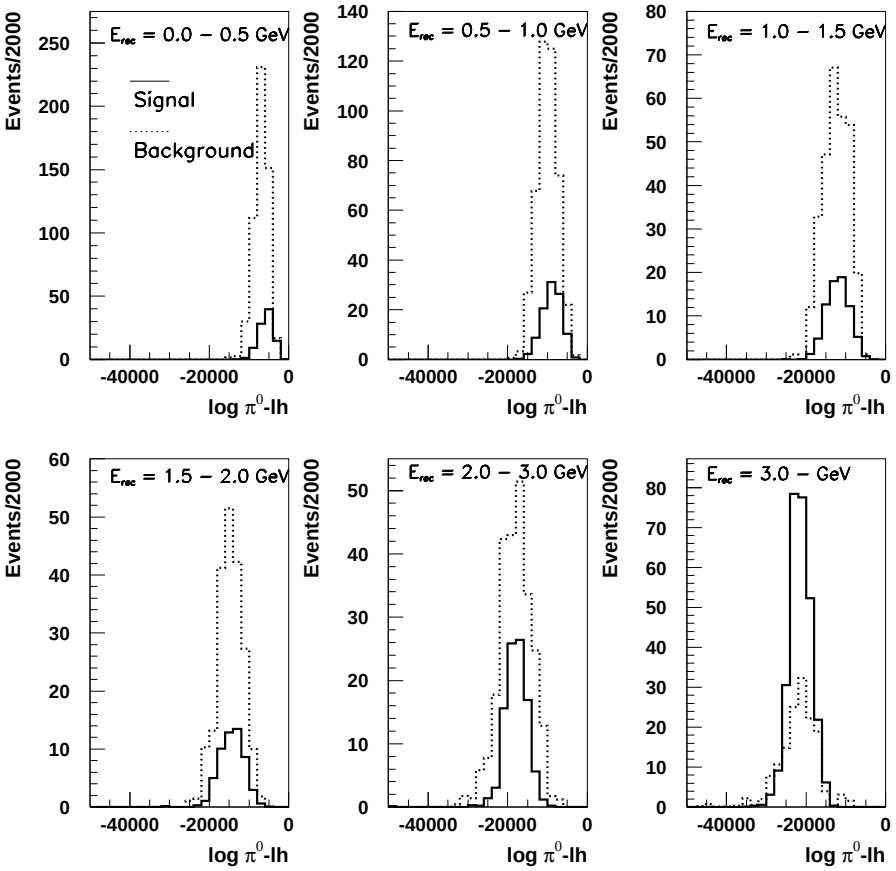

FIG. 11: $\log \pi^0$-lh: The distributions of the π^0-likelihood of the primary e-like ring. The distribution in solid line is for the signal and that in dotted line is for the background.

V. DISCRIMINATOR: LIKELIHOOD FUNCTION AND LIKELIHOOD RATIO

A series of cuts on the variables described in the previous section reduce the background. However, too many cuts reduce the signal level significantly. The problem is that none of the variables can individually separate the signal from the background very well. In this situation one of the simplest techniques is to define a likelihood function using variables that can, at some level, distinguish the signal events from the background events. We have shown that the nine variables described above are distributed differently depending on the origin of the candidate events selected as the signal (on whether they are from the signal or background), even when these difference are small. As we will see, an accumulation of relatively small differences can make a bigger difference.

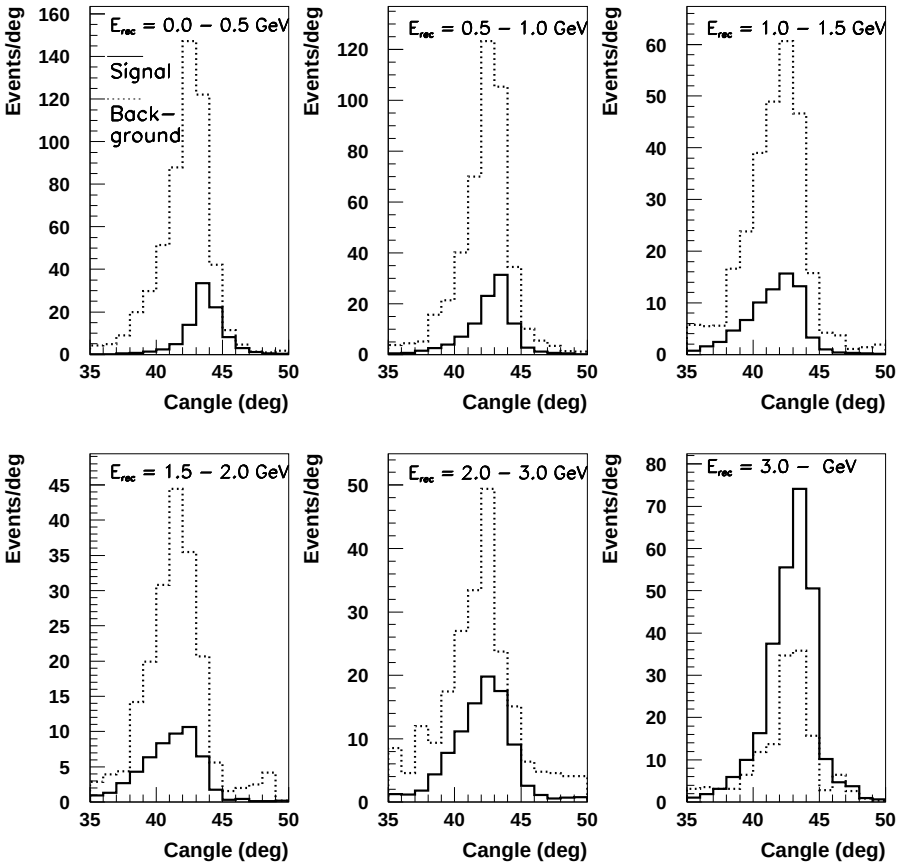

FIG. 12: Cangle: The distributions of the measured Cherenkov angle of the primary e-like ring. The distribution in solid line is for the signal and that in dotted line is for the background.

From each distribution shown in Figs. 5-13, a probability is calculated for an event to have value of each variable j for the signal p_j^s and for the background p_i^b. Then the log-likelihood is defined by $\log L_s = \Sigma_{j=1,..,9} \log(p_j^s)$ as signal and by $\log L_b = \Sigma_{i=1,..,9} \log(p_i^b)$ as background. Due to lack of statistics of Monte Carlo events, especially in higher E_{rec} region, the distributions of the nine variables must be divided into relatively coarse E_{rec} bins. The binning chosen is as used in Figs. 5-13, specifically: 0.0 - 0.5 GeV, 0.5 - 1.0 GeV, 1.0 - 1.5 GeV, 1.5 - 2.0 GeV, 2.0 - 3.0 GeV, and above 3.0 GeV. Finally, the difference between two log-likelihoods, $\Delta \log L = \log L_b - \log L_s$, is calculated to decide upon whether an event is more signal-like or background-like. Fig. 14 shows $\Delta \log L$ distributions for different E_{rec} regions for the signal events (solid line) and the background events (dotted

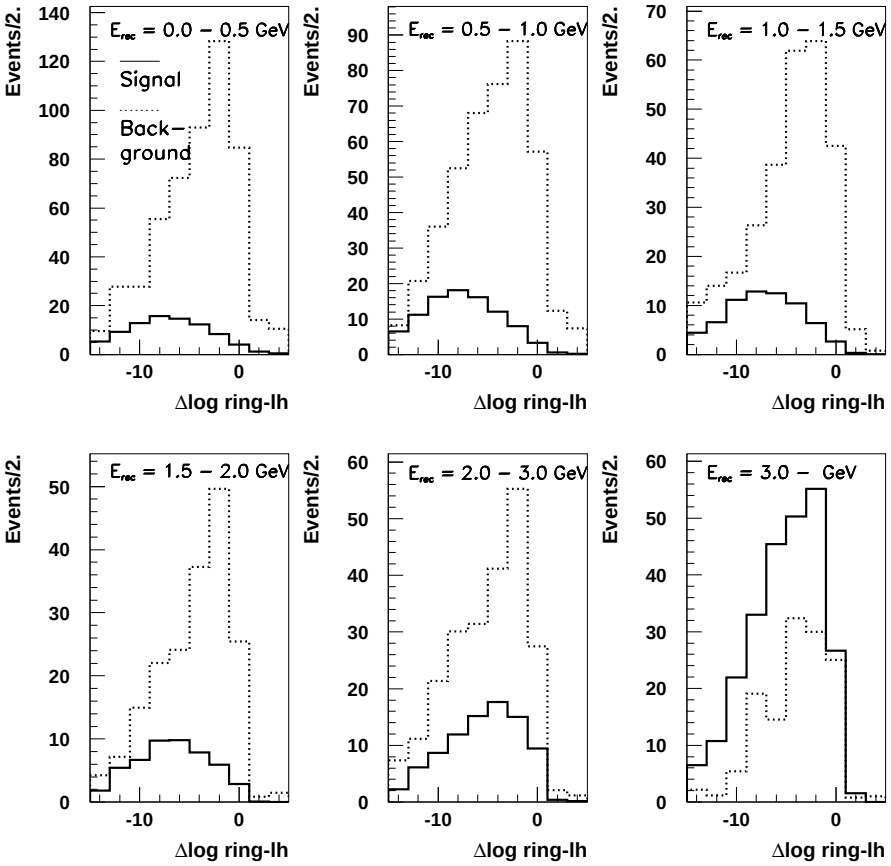

FIG. 13: $\Delta \log$ ring-lh: The distributions of difference in log-likelihood of two hypotheses on the number of Cherenkov ring in an event: there is only one Cherenkov ring or more. If this difference is negative, the event is less likely to have an additional ring. The distributions in solid line are for the signal and that in dotted line are for the background.

line). The smaller $\Delta \log L$ is, the more likely an event is a signal event. It is clearly seen that the $\Delta \log L$ distribution of the signal events differ very much from that of background events over wide range of E_{rec}.

The decision on the event classification as signal or background is done by setting a boundary value on $\Delta \log L$: if the value of $\Delta \log L$ is less (greater) than this boundary value, the event is considered signal-like (background-like). As the distributions of the nine variables used to define the likelihood depend on E_{rec}, so does the distribution of $\Delta \log L$. Therefore, in order not to change the energy spectrum unnecessarily, we adopt a strategy

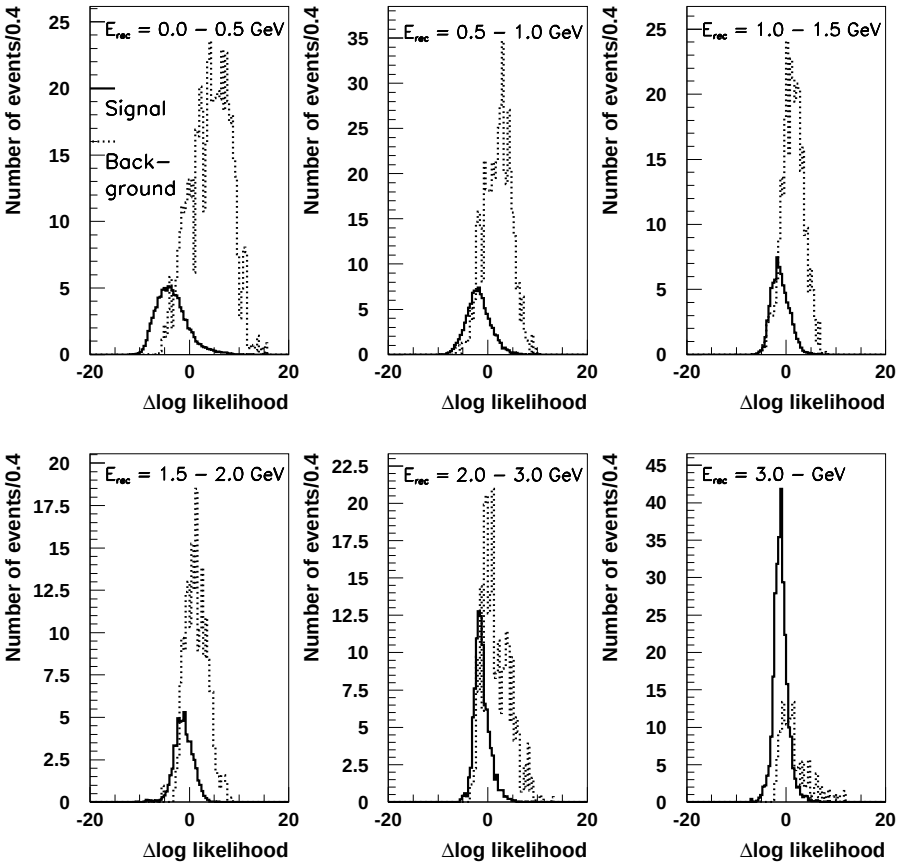

FIG. 14: The distributions of the difference in log-likelihood of two hypotheses on the origin of events: signal vs. background. The distributions in solid line are for the signal and that in dotted line are for the background.

to keep the signal detection efficiency constant over a wide range of E_{rec} by changing the boundary value that divides the event classification according to E_{rec}.

VI. RECONSTRUCTED NEUTRINO ENERGY DISTRIBUTIONS WITH A CUT ON $\Delta \log L$

To show the effectiveness of the cut on $\Delta \log L$, we now set the boundary values that define whether an event is signal-like or background-like for a given E_{rec} such that either 40% or 50% of signal events are retained after the cut. This cut is applied to both the signal

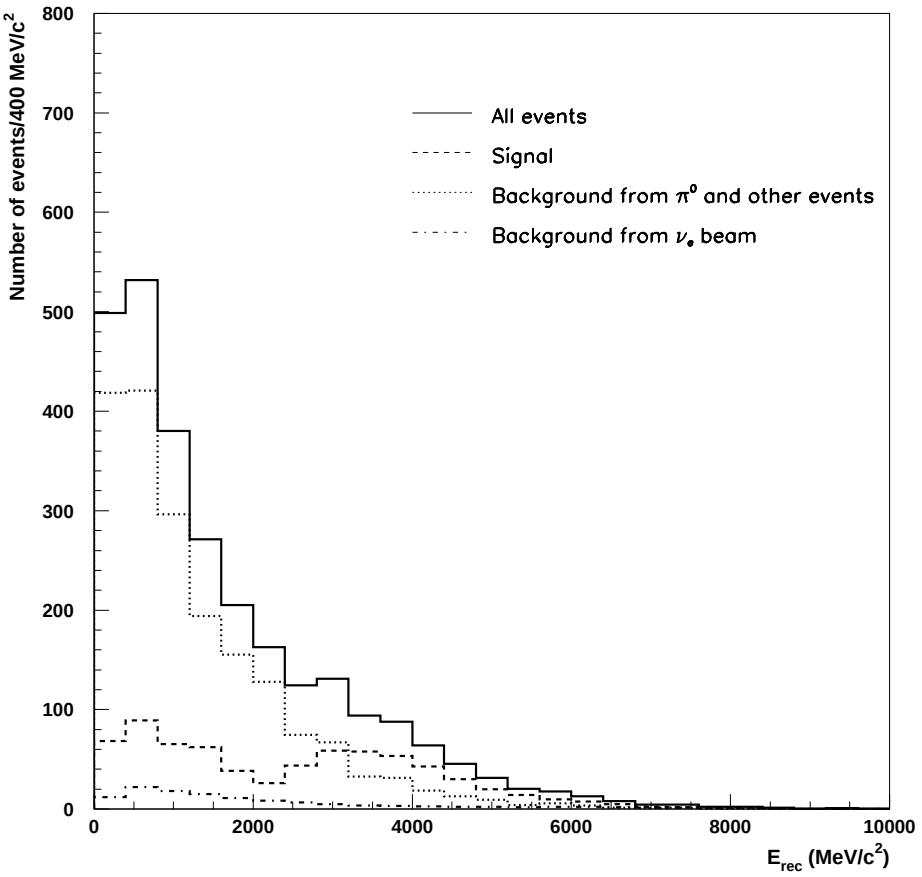

FIG. 15: The distribution of the reconstructed neutrino energy with the standard Super-Kamiokande cuts before the cut on $\Delta \log L$ is applied. The distribution in dashed line is for the signal and those in dotted (dash-dotted) line is for the background 1(2). $\delta_{CP} = +45^o$ and the baseline is 2,540 km.

and background events.

First we show how well the traditional analysis represented by the standard SK-I analysis codes can remove the background contribution. Fig. 15 shows the E_{rec} distributions of the signal (dashed line), of the background (background 1) arising mostly from neutral current interactions (dotted line), and of the irreducible background (background 2) arising from the ν_e contamination in the neutrino beam (dash-dotted line). The signal is overwhelmed by the background, especially in low energy region. In this case, we find 700 signal events, 1,877 events from background 1, and 127 events from background 2.

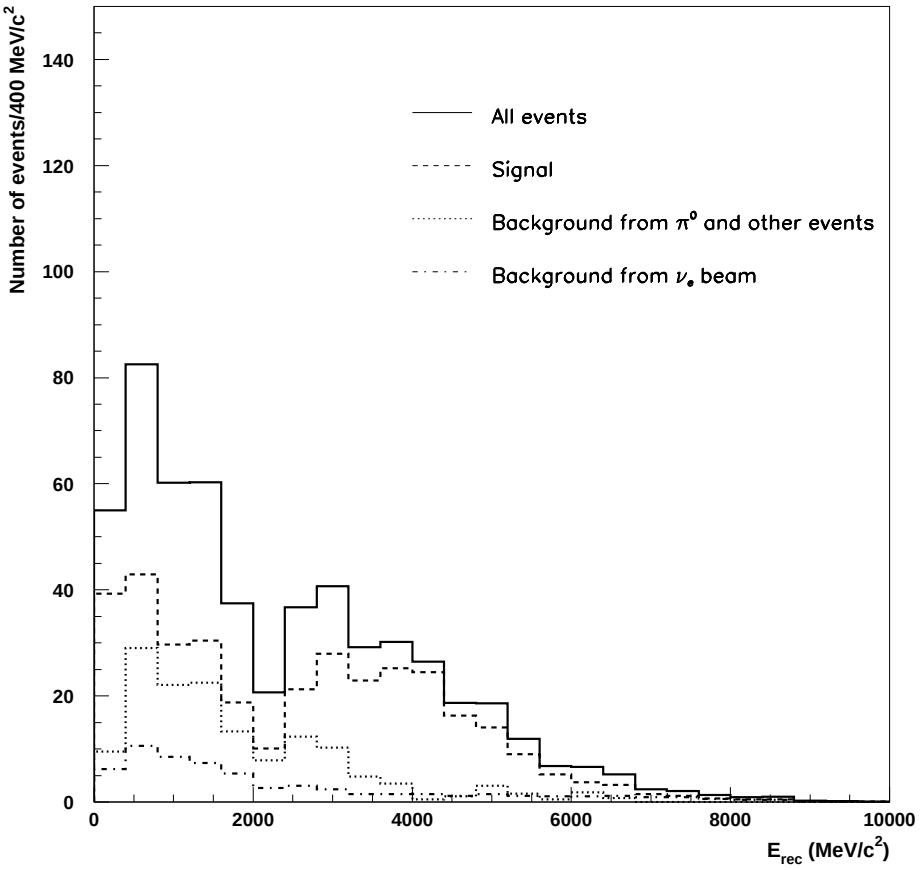

FIG. 16: The distribution of the reconstructed neutrino energy, in addition to the standard Super-Kamiokande cuts, the cut on $\Delta \log L$ is applied in such a way to retain 50% of the signal events survive by this cut. The distribution in dashed line is for the signal and that in dotted (dash-dotted) line is for the background. $\delta_{CP} = +45^o$ and the baseline is 2,540 km.

If we retain 50% of the signal events after the cut on $\Delta \log L$, the contribution from background 1 is much more reduced as shown in Fig. 16. In this case, we found 349 signal, 145 background 1, and 62 background 2 events.

Furthermore if we tighten the cut slightly to retain only 40% of the signal events, again the background 1 events are much more reduced with only a small reduction of the signal as shown in Fig. 17. In this case, we find 280 signal, 87 background 1, and 49 background 2 events.

The analyses presented here use nine variables to define the likelihood function. The use

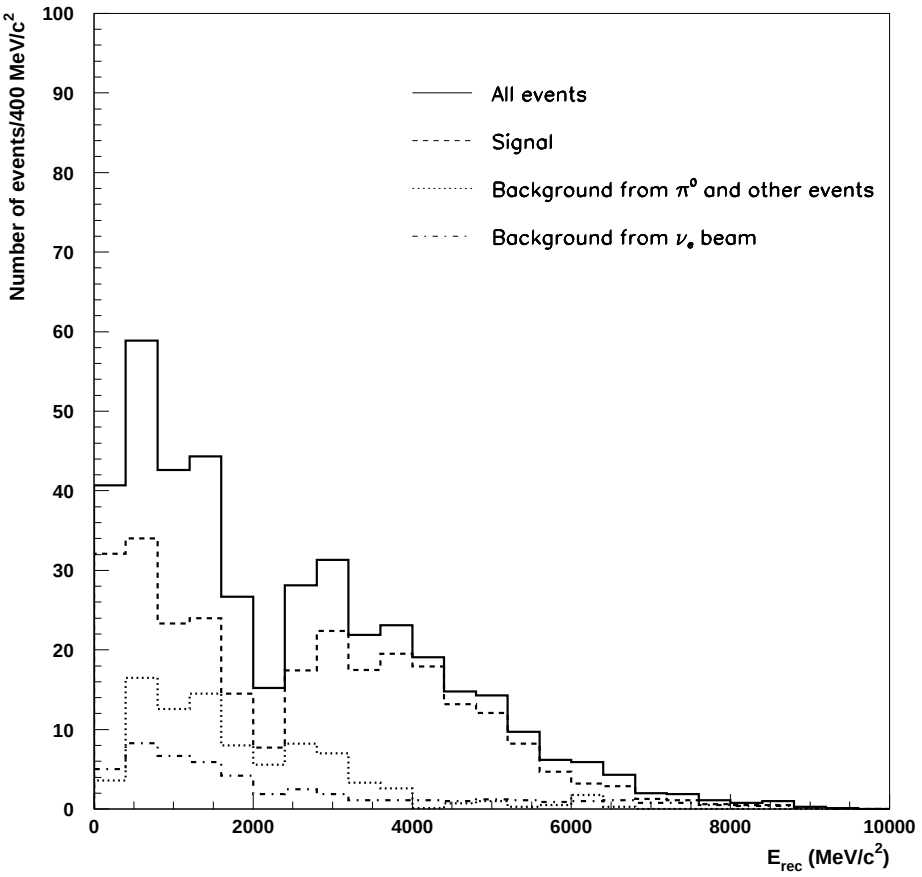

FIG. 17: The distribution of the reconstructed neutrino energy, in addition to the standard Super-Kamiokande cuts, the cut on $\Delta \log L$ is applied in such a way to retain 40% of the signal events survive by this cut. The distribution in dashed line is for the signal and that in dotted (dash-dotted) line is for the background 1(2). $\delta_{CP} = +45^o$ and the baseline is 2,540 km.

of these variables is justified by examining how much the signal-to-background (S/B) ratio changes from the case where all the nine variables are used to the case where each variable is removed from the definition of the likelihood in turn. Table I summarizes the numbers of events from different sources together with the S/B ratio for which only the contribution from background 1 is used. For this table, the cut on $\Delta \log L$ is used to retain 40% of the signal events by this cut.

The fact that the S/B ratio always decreases when one variable is removed from the definition of the likelihood confirms that the use of the nine variables is justified.

TABLE I: Summary of the numbers of the signal and background events, and the signal-to-background ratio using events from background 1 with the cut on $\Delta \log L$ to retain 40% of the signal events. The CP-violating phase is assumed to be 45^o and the baseline is 2,540 km.

Variable removed	Sig	Bkg 1	Bkg 2	Sig/Bkg 1
None	280	87	49	3.22
Δ log π^0-lh	281	102	50	2.75
Q/E	281	94	49	2.98
log π^0-lh	278	94	51	2.98
Δ log pid-lh	277	94	46	2.96
E_{frac}	281	98	49	2.85
$m_{\gamma\gamma}$	280	105	50	2.66
cosθ	279	101	49	2.76
Cangle	280	98	49	2.86
Δ log ring-lh	277	95	49	2.93

VII. E_{rec} DISTRIBUTIONS AND CP-VIOLATING PHASE δ_{CP}

In the previous section we showed that, with a set of appropriate cuts, the background contribution can be suppressed down to a reasonable level, while retaining enough statistics for the signal. In this section, we see whether this set of the cuts is still useful for values of the CP-violating phase δ_{CP} other than $+45^o$. The cut on $\Delta \log L$ is set to retain 40% of the signal. Fig. 18 shows the E_{rec} distribution of the signal (dashed line), background 1 (dotted line) and background 2 (dash-dotted line) for $\delta = +135^o$. Similarly Figs. 19, 20 and 21 show the E_{rec} distributions for $\delta = 0^o, -45^o$, and -135^o, respectively. Table II lists the numbers of events from the signal, background 1 and background 2 for different values of δ_{CP}.

In all cases, there are more signal events than background events. In the worst case with $\delta_{CP} = -45^o$ the ratio signal/(background 1 + background 2) is 1.18, while in the best case with $\delta_{CP} = +135^o$ the ratio is 2.78.

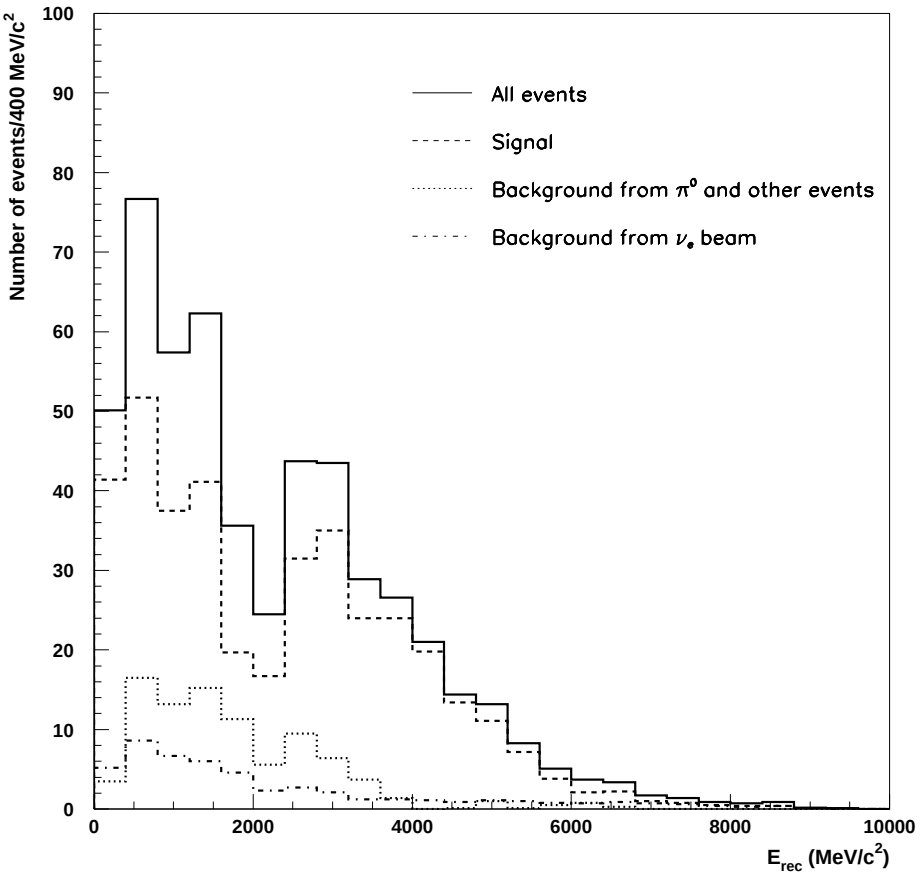

FIG. 18: The distribution of the reconstructed neutrino energy, in addition to the standard Super-Kamiokande cuts, the cut on $\Delta \log L$ is applied in such a way to retain 40% of the signal events survive by this cut. The distributions in dashed line is for the signal and that in dotted (dash-dotted) line is for the background 1(2). $\delta_{CP} = +135^o$ and the baseline is 2,540 km.

VIII. E_{rec} DISTRIBUTIONS AND BASELINE

It is interesting to see how the baseline will change the results of similar analyses presented in the preceeding section. In this section, the cut on $\Delta \log L$ is used to retain 40% of signal and the baseline is assumed to be 1,480 km (Fermilab to Henderson Mine). Figs. 22-26 show the E_{rec} distribution of the signal (dashed line), background 1 (dotted line) and background 2 (dash-dotted) for $\delta = +135^o, +45^o, 0^o, -45^o$, and -135^o, respectively. Table III lists the numbers of events from the signal, background 1 and background 2 for different values of

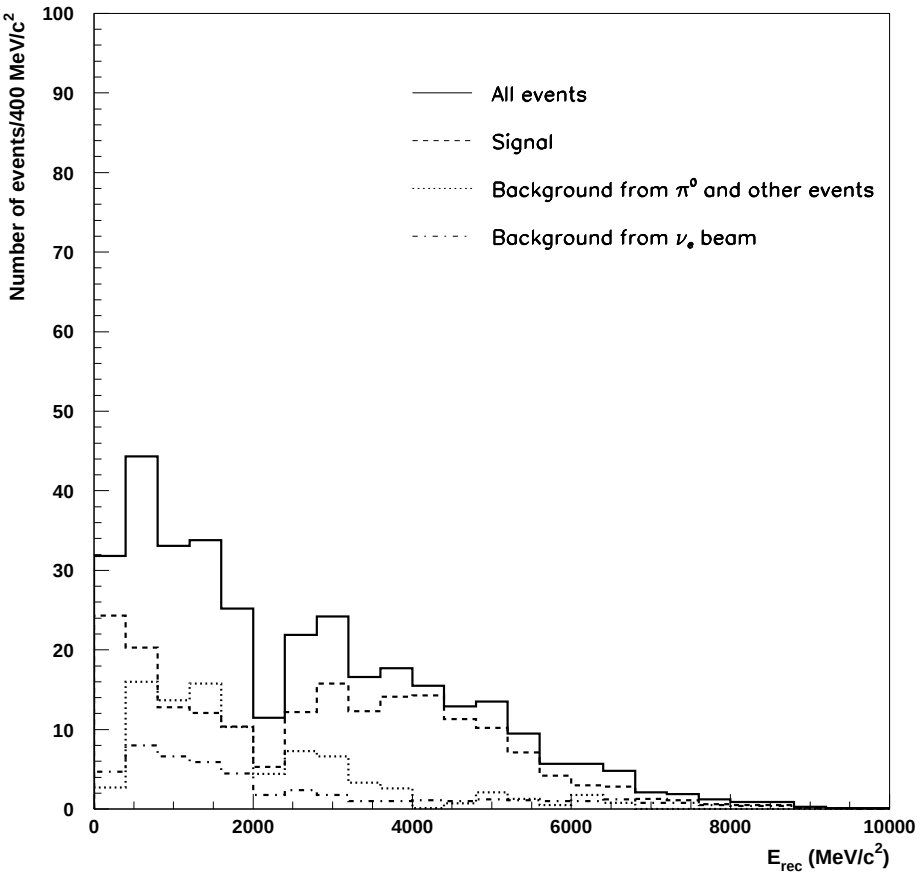

FIG. 19: The distribution of the reconstructed neutrino energy, in addition to the standard Super-Kamiokande cuts, the cut on $\Delta \log L$ is applied in such a way to retain 40% of the signal events survive by this cut. The distribution in dashed line is for the signal and that in dotted (dash-dotted) line is for the background 1(2). $\delta_{CP} = 0^o$ and the baseline 2,540 km.

δ_{CP}.

With a baseline of 1,480 km, although the ratio signal/(background 1 + background 2) is reduced from the case with a longer baseline of 2,540 km for all the vlaues of δ_{CP} (in the worst case with $\delta_{CP} = -45^o$ the ratio is 0.92 and in the best case with $\delta_{CP} = +45^o$ the ratio is 1.87), a significant increase in statistics in all the cases will reduced the statistical error and improve the sensitivity to δ_{CP} and to other oscillation parameters. Furthermore we could apply an additional cut such as the one on the distance to the PMT surface from the recosntructed vertex position, which will be described later in this paper, to enhance

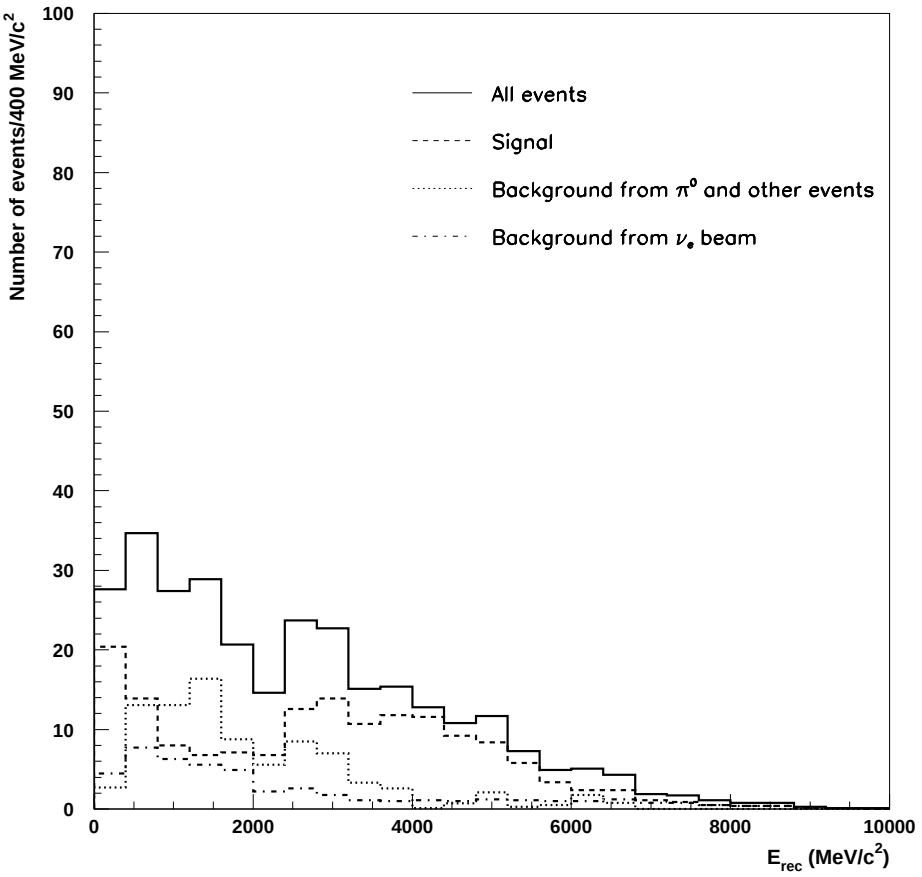

FIG. 20: The distribution of the reconstructed neutrino energy, in addition to the standard Super-Kamiokande cuts, the cut on $\Delta \log L$ is applied in such a way to retain 40% of the signal events survive by this cut. The distribution in dashed line is for the signal and that in dotted (dash-dotted) line is for the background. $\delta_{CP} = -45^o$ and the baseline is 2,540 km

the ratio signal/background 1.

IX. SOURCES OF BACKGROUND EVENTS

It is important to know where the background events come from. Information such as the true energy of neutrinos and nature of the interactions of neutrinos that produce the background events is very useful for designing the neutrino beam for a very long baseline neutrino experiment.

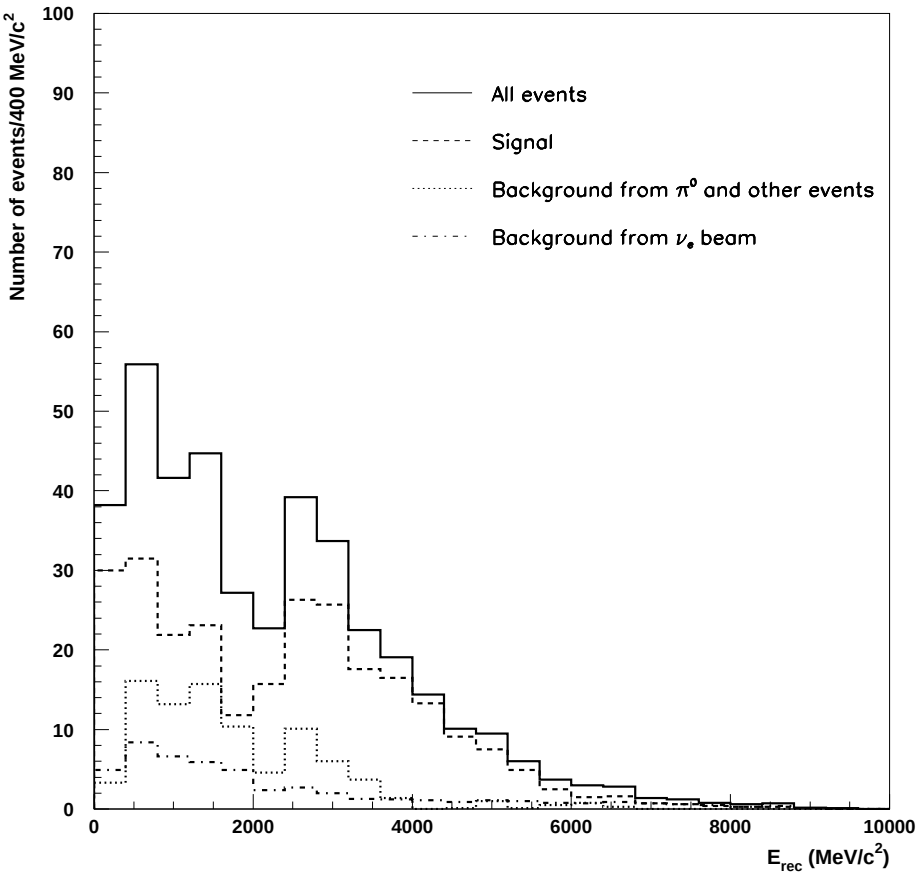

FIG. 21: The distribution of the reconstructed neutrino energy, in addition to the standard Super-Kamiokande cuts, the cut on $\Delta \log L$ is applied in such a way to retain 40% of the signal events survive by this cut. The distribution in dashed line is for the signal and that in dotted (dash-dotted) line is for the background 1(2). $\delta_{CP} = -135^o$ and the baseline is 2,540 km.

Figs. 27-28 show the true neutrino energy distributions of the signal, background 1 and background 2 events for the baseline of 2,540 km and 1,480 km, respectively. These events are chosen with the $\Delta \log L$ cut that retains 40% of the signal events after the first set of the cuts (the standard Super-kamiokande cuts).

For the most of the results presented in this report, we apply the cut on the neutrino energy at 10 GeV. To justify this cut, we checked how much more the background contribution would increase if we allowed events produced by neutrinos with energies greater than 10 GeV and less than 15 GeV. For these additional events we fix the weight value, which

TABLE II: Summary of the numbers of the signal and background events for different values of δ_{CP} using events from background 1 with the cut on $\Delta \log L$ to retain 40% of the signal events with the baseline of 2,540 km.

δ_{CP}	Sig	Bkg 1	Bkg 2
$+135^o$	386	89	50
$+45^o$	279	87	49
0^o	197	90	48
-45^o	159	87	48
-135^o	263	87	49

TABLE III: Summary of the numbers of signal and background events for different values for δ_{CP} using events from background 1 with the cut on $\Delta \log L$ to retain 40% of the signal events with the baseline of 1,480 km.

δ_{CP}	Sig	Bkg 1	Bkg 2
$+135^o$	646	238	142
$+45^o$	699	233	141
0^o	498	230	140
-45^o	357	247	142
-135^o	609	237	142

converts the atmospheric ν_e energy spectrum to that of the very long baseline wideband neutrino beam, at the value for the ν_μ energy of 10 GeV. The atmospheric ν_e flux times the ν_e cross section decreases by about 60% from 10 GeV to 15 GeV while that for the wideband ν_μ beam by about 50% in this energy region. Therefore the atmospheric ν_e and ν_μ spectrum are only slightly softer than the wideband ν_μ spectrum from 10 GeV to 15 GeV. This argument, therefore, gives a reasonable estimate of the extra contribution from high energy neutrinos. All the neutrino oscillation parameters are the same as in the case with $\delta_{CP} = +45^o$, the baseline of 2,450 km, and the 40% $\Delta \log L$ cut. The numbers of the signal, background 1, and background 2 events accepted are 281, 91 and 49, respectively, which are to be compared with 279 for the signal, 87 for the background 1 and 49 for the background

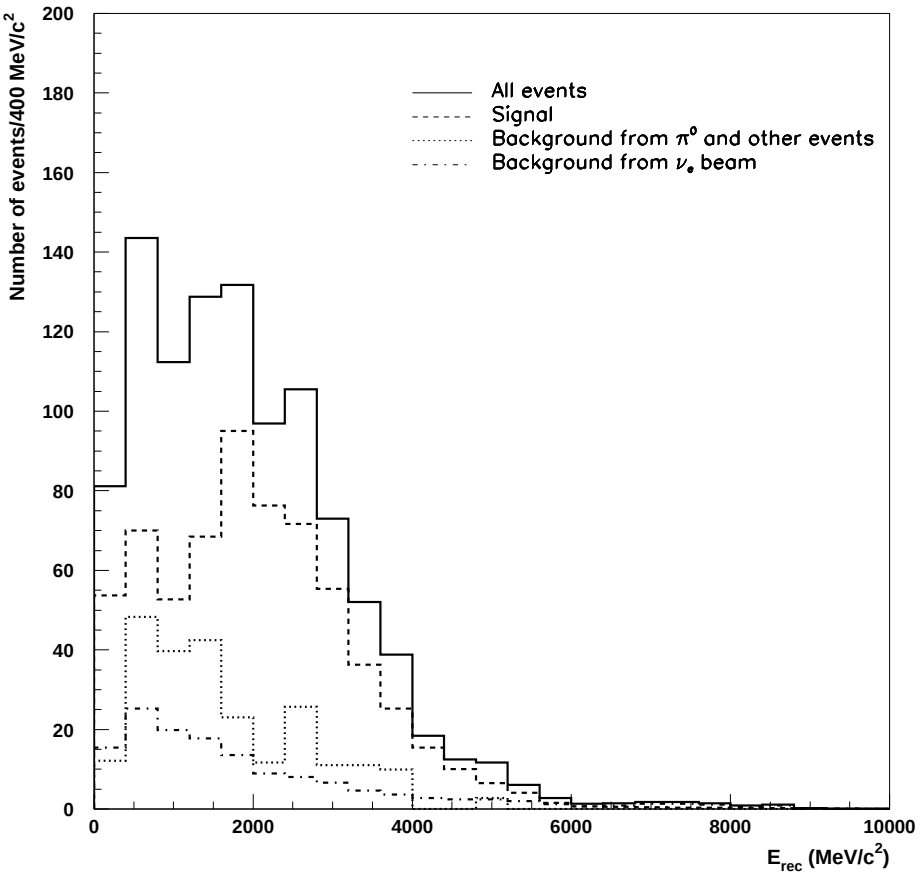

FIG. 22: The distribution of the reconstructed neutrino energy, in addition to the standard Super-Kamiokande cuts, the cut on $\Delta \log L$ is applied in such a way to retain 40% of the signal events survive by this cut. The distributions in dashed line is for the signal and that in dotted (dash-dotted) line is for the background 1(2). $\delta_{CP} = +135^o$ and the baseline is 1,480 km.

2 with the neutrino energy cut at 10 GeV. Thus the percent increases in the number of the signal, background 1 and background 2 events are 1%, 4%, and 0%, respectively.

Tables IV and V summarize the interactions of the candidate events that pass all the cuts with 40% efficiency for the $\Delta \log L$ cut with the baseline of 2,540 km and 1,480 km, respectively. In these tables, CC and NC stand for charged and neutral current interactions; π^0,$\pi^{\pm}$, and $n\pi$ stand for single π^0, single $\pi^{\pm}$ and multiple π production, respectively. Note that the tables contain no contribution from neutral current interactions for the signal events by definition.

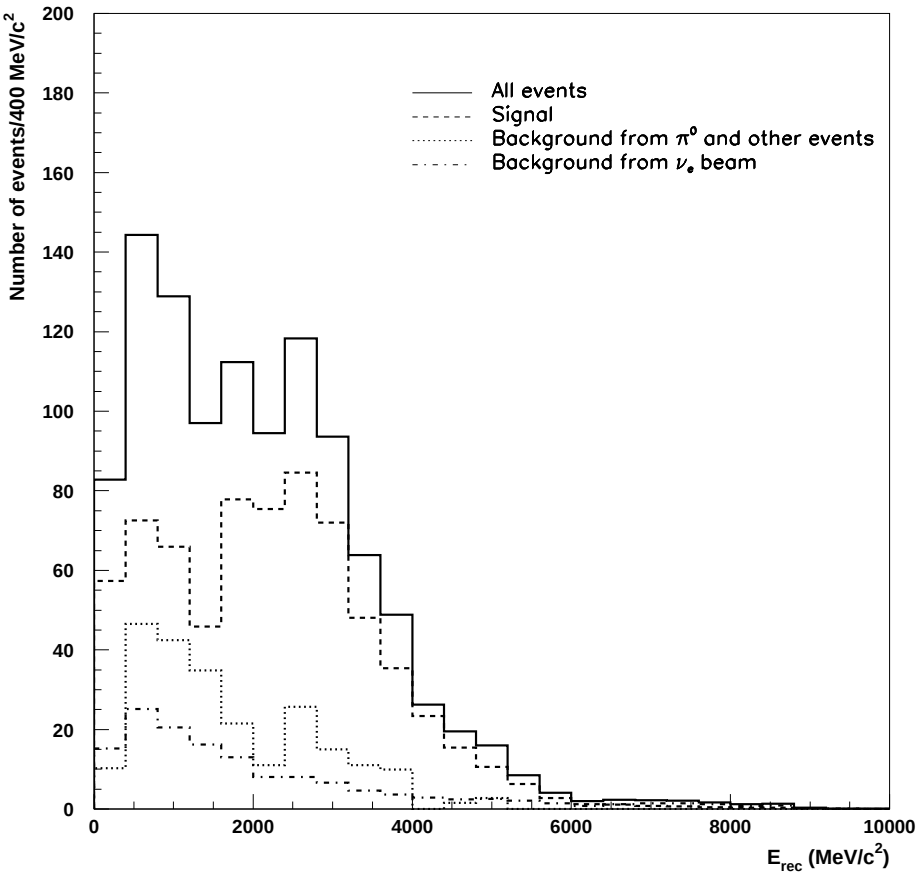

FIG. 23: The distribution of the reconstructed neutrino energy, in addition to the standard Super-Kamiokande cuts, the cut on $\Delta \log L$ is applied in such a way to retain 40% of the signal events survive by this cut. The distributions in dashed line is for the signal and that in dotted (dash-dotted) line is for the background. $\delta_{CP} = +45^o$ and the baseline is 1,480 km.

X. DETECTOR SIZE AND GRANULARITY

It is interesting to see what effect the detector size has on the performance of the *POLfit*. Although the results reported so far are based on the analyses of the Monte Carlo events generated for the Super-Kamiokande detector with 40% PMT coverage, we can make some assessment on the effect by imposing a cut on the distance to the PMT surface from the π^0 production point in the flight direction of the π^0 (dmin). For this study we use single π^0 events produced by neutral current interactions. When the π^0 energy is greater than about 1

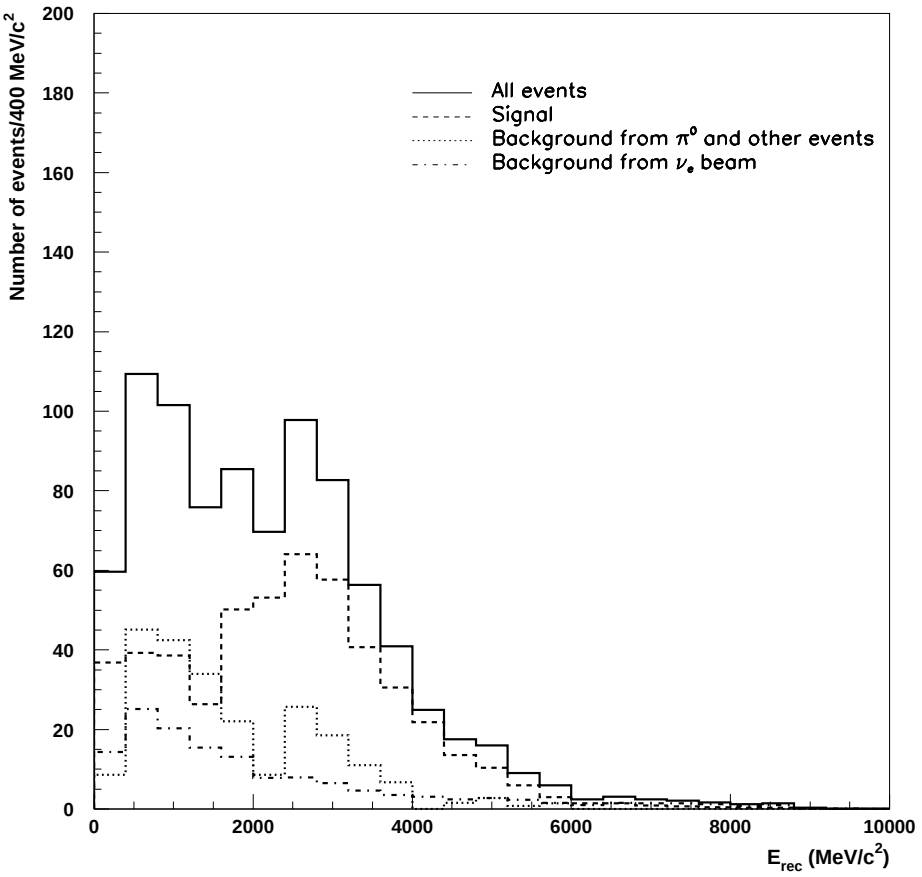

FIG. 24: The distribution of the reconstructed neutrino energy, in addition to the standard Super-Kamiokande cuts, the cut on $\Delta \log L$ is applied in such a way to retain 40% of the signal events survive by this cut. The distributions in dashed line is for the signal and that in dotted (dash-dotted) lines is for the background. $\delta_{CP} = 0^o$ and the baseline is 1,480km.

GeV, the minimum opening angle of two photons becomes 20^o or less. If dmin increases, the number of PMTs that detect Cherenkov photons from the π^0 photons increases (granularity), although each PMT receives less Cherenkov light due to increase in the Cherenkov cone size and in amount of Cherenkov photon interactions with water such absorption and scattering (attenuation).

Figure 29 shows the π^0 detection efficiency as a function of the opening angle for dmin ranges: 5 m - 10 m, 15 m - 20 m, and 25 m - 30 m. It is clearly seen that when the opening angle is smaller (less than 60^o), the efficiency is improved as the distance to the

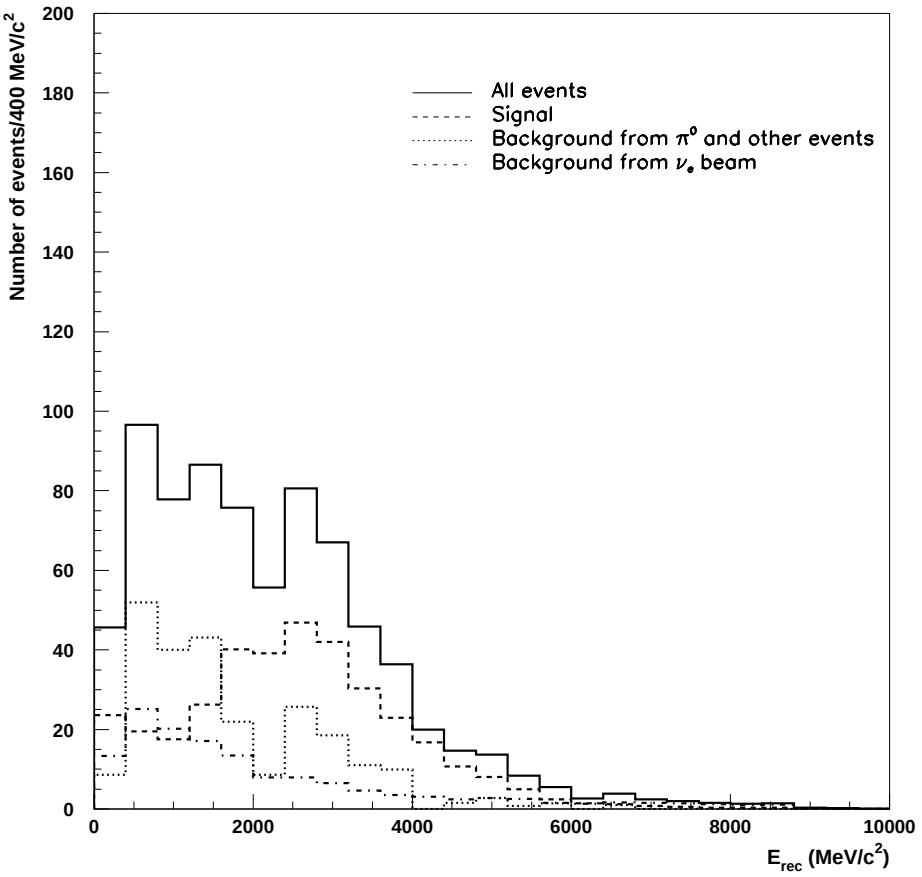

FIG. 25: The distribution of the reconstructed neutrino energy, in addition to the standard Super-Kamiokande cuts, the cut on $\Delta \log L$ is applied in such a way to retain 40% of the signal events survive by this cut. The distribution in dashed line is for the signal and that in dotted (dashed-dotted) line is for the background 1(2). $\delta_{CP} = -45^o$ and the baseline is 1,480 km.

PMT surface in the π^0 direction increases. Note that for the opening angles of smaller than 60^o, the π^0 detection efficiency seems more or less independent of dmin. This indicates that the granularity of the detector in terms of the PMT density is an important factor for improving the π^0 detection efficiency. It also seems that the effect of light attenuation is not a major issue. Therefore, for the same PMT coverage using the same PMTs, a larger detector performs better in reconstructing the π^0 events than a smaller one until either light attenuation or PMT's cathode size becomes a problem.

Granularity, that is the number of PMTs imaging a ring, is also important to reducing

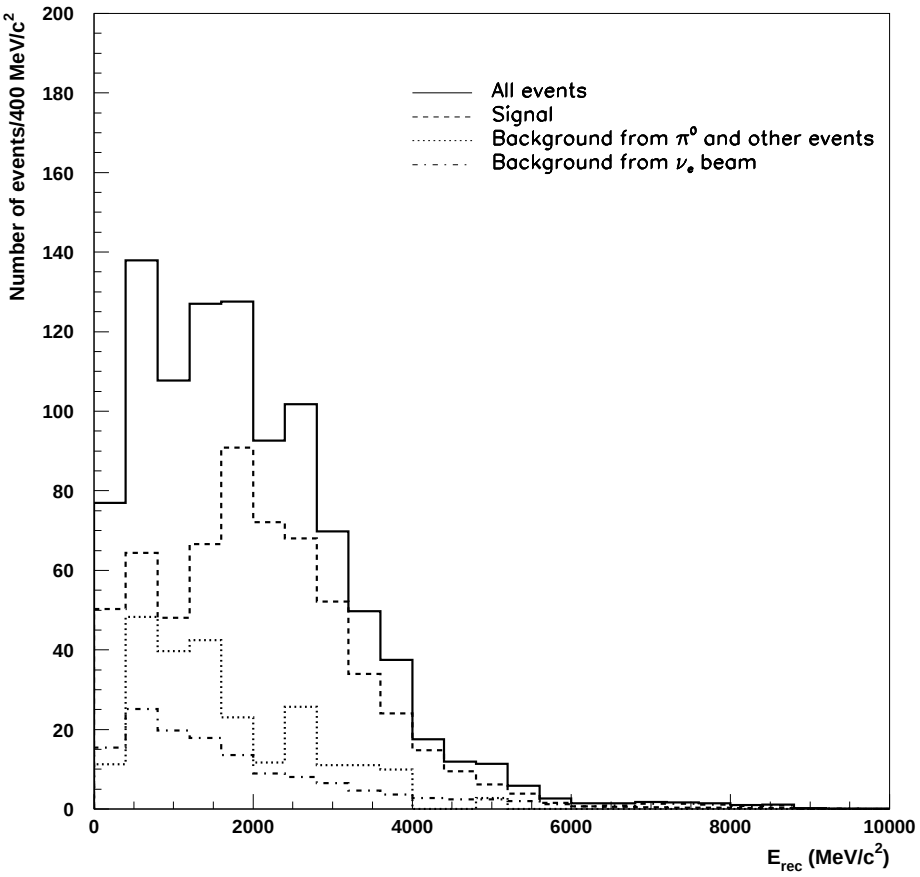

FIG. 26: The distribution of the reconstructed neutrino energy, in addition to the standard Super-Kamiokande cuts, the cut on $\Delta \log L$ is applied in such a way to retain 40% of the signal events survive by this cut. The distribution in dashed line is for the signal and that in dotted (dash-dotted) line is for the background 1(2). $\delta_{CP} = -135^o$ and the baseline is 1,480 km.

backgrounds. For example, a charged pion traveling in the same direction as a photon or electron will produce an event with overlapping rings. If this event is very close to the wall the charged pion may make it to the outer (veto) detector and be detected and the event will be cut. Otherwise the only way to detect it is through resolving the double ring pattern. The ability to resolve this depends on the number of PMTs imaging the pattern. This source of background can be seen in Table V in the significant contribution from CC events $\nu_e + N \rightarrow e^- + N' + \pi^{\pm}$ identified as a single e-like events.

To examine how sensitive the S/B ratio is to the detector size and its granularity, we

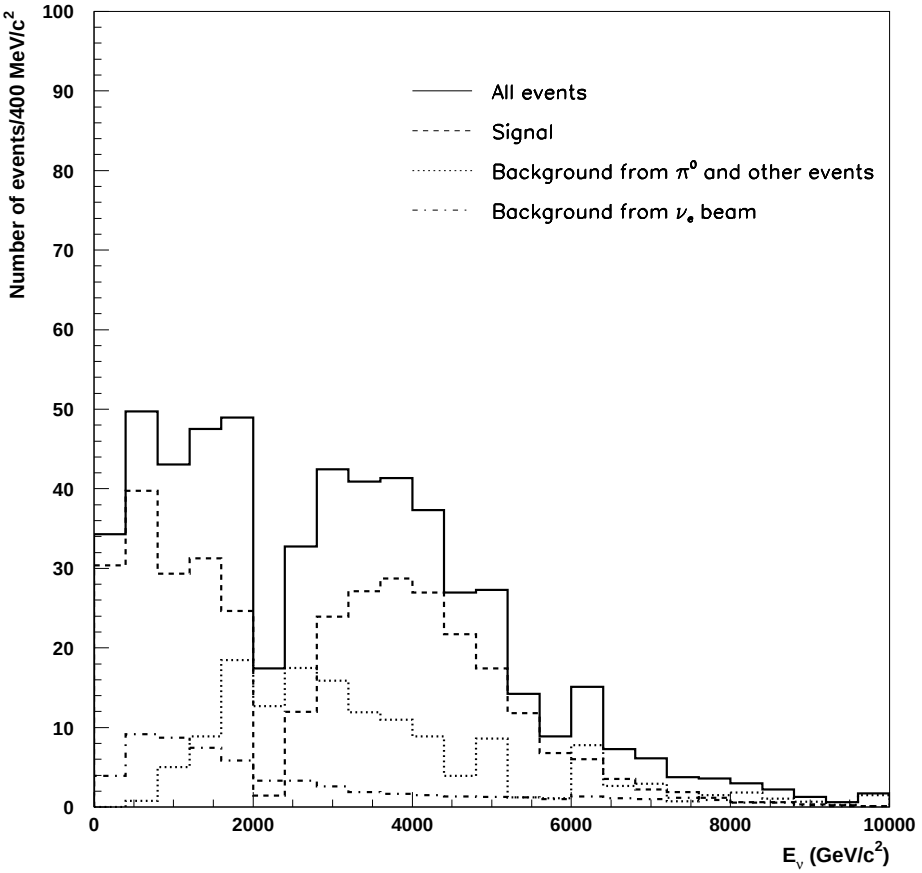

FIG. 27: The distribution of the true neutrino energies that produced the signal, background 1 and background 2 events. In addition to the standard Super-Kamiokande cuts, the cut on $\Delta \log L$ is applied in such a way to retain 40% of the signal events survive by this cut. The distribution in dashed line is for the signal and that in dotted (dash-dotted) is for the background 1(2). $\delta_{CP} = +45^o$ and the baseline is 2,540 km.

apply a cut on the distance to the PMT surface from the reconstructed vertext position and in the direction of the primary e-like ring. This cut mimics, to a certain degree, the effects of detector size and in the detector granularity. As more distance from the wall is required the event sample is biased to more closely resemble samples taken from larger detectors where the available phase space prefers a larger average distance between vertex and wall.

When this distance cut is applied to events passing the previously described cuts by requiring the distance be 20 m or larger, the S/B ratio changes from 1.4 to 3.8 for events with

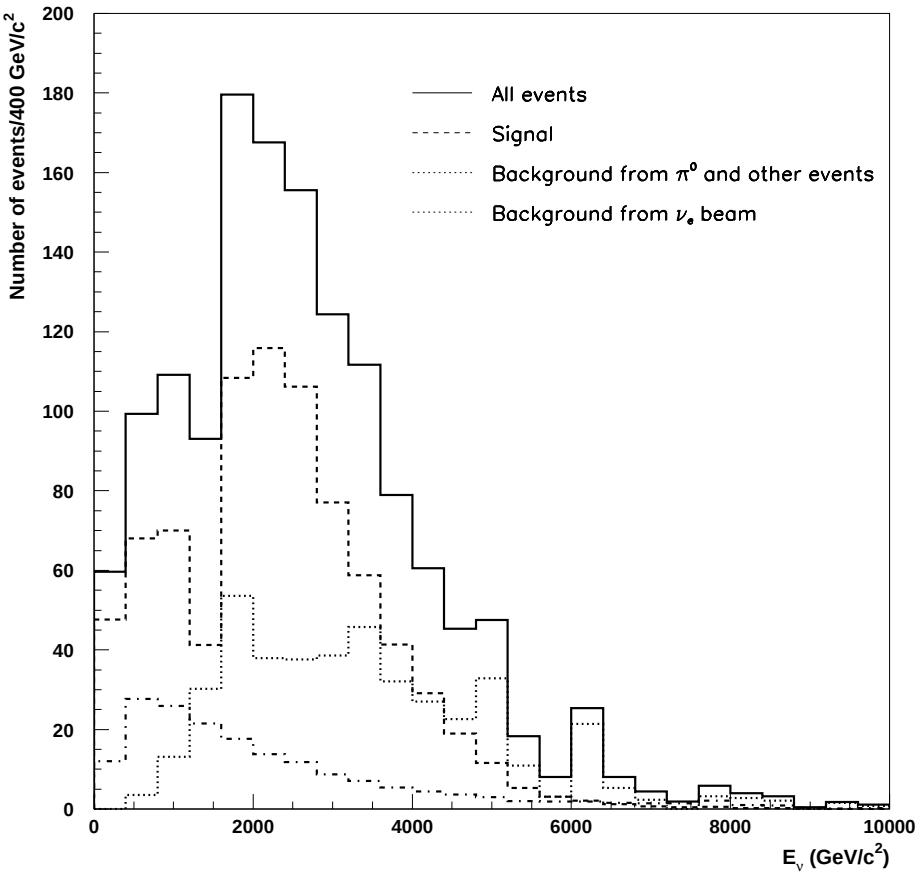

FIG. 28: The distribution of the true neutrino energies that produced the signal, background 1 and background 2 events. In addition to the standard Super-Kamiokande cuts, the cut on $\Delta \log L$ is applied in such a way to retain 40% of the signal events survive by this cut. The distribution in dashed line is for the signal and that in dotted (dash-dotted) is for the background 1(2). $\delta_{CP} = +45^o$ and the baseline is 1,480 km.

$E_{rec} \leq 1.2$ GeV, while for events with 2 GeV $\leq E_{rec} < 4$ GeV the S/B ratio essentially stays the same. Note that for this analysis we use the Monte Carlo events with $\delta_{CP} = +45^o$. The large improvement in the S/B ratio for events with $E_{rec} \leq 1.2$ GeV results from an increase in the number of PMTs (pixels) in a Cherenkov ring. This improvement is significant in the energy region $E_{rec} \leq 1.2$ GeV as the contribution from the neutral current events is reduced to a level as low as that from the irreducible background. This improvement, however, is not realized for events with 2 GeV $\leq E_{rec} < 4$ GeV presumably because in this energy region

TABLE IV: Summary of the percent contributions from events produced by different interactions for signal events and for background 1 events are summarized in the cases for $\delta_{CP} = +45^o$, the cut on $\Delta \log L$ to retain 40% of the signal events and the baseline of 2,540 km.

Interaction	E_{rec} range (GeV)					
Sig	0.0-0.5	0.5-1.0	1.0-1.5	1.5-2.0	2.0-3.0	3.0-
CC QE	68%	63%	50%	65%	23%	37%
CC π^0	2%	2%	3%	2%	4%	4%
CC $\pi^{\pm}$	9%	12%	22%	9%	30%	24%
CC $n\pi$	1%	3%	3%	4%	21%	12%
CC others	0%	1%	2%	1%	8%	5%
Bkg 1	0.0-0.5	0.5-1.0	1.0-1.5	1.5-2.0	2.0-3.0	3.0-
CC QE	7%	5%	6%	1%	0%	0%
CC π^0	0%	1%	4%	6%	4%	0%
CC $\pi^{\pm}$	3%	5%	0%	1%	0%	0%
CC $n\pi$	0%	0%	3%	6%	20%	3%
CC others	0%	0%	0%	0%	0%	0%
NC π^0	23%	53%	59%	59%	18%	0%
NC $\pi^{\pm}$	63%	10%	6%	0%	0%	0%
NC $n\pi$	0%	13%	5%	16%	55%	92%
NC others	4%	14%	16%	12%	3%	5%

multi-pion events are the major background. This observation is also true if the minimum distance is set even at 10 or 15 m, although the improvement in the S/B ratio is less than the case of the 20 m cut. For a SK-I sized detector, this 20 m cut reduces the number of the signal events by 41%. However, if the detector is larger, this loss of efficiency can be greatly reduced. In other words, for a given detector size, the finer granularity, not necessarily the number of Cherenkov photons collected by individual PMT, improves the S/B ratio.

TABLE V: Summary of the percent contributions from events produced by different interactions for signal events and for background 1 events are summarized in the cases for $\delta_{CP} = +45^o$, the cut on $\Delta \log L$ to retain 40% of the signal events and the baseline of 1,480 km.

Interaction	E_{rec} range (GeV)					
Sig	0.0-0.5	0.5-1.0	1.0-1.5	1.5-2.0	2.0-3.0	3.0-
CC QE	80%	78%	36%	53%	58%	55%
CC π^0	3%	3%	9%	5%	4%	5%
CC $\pi^{\pm}$	15%	15%	39%	30%	27%	27%
CC $n\pi$	1%	3%	14%	10%	9%	10%
CC others	0%	2%	4%	2%	5%	4%
Bkg 1	0.0-0.5	0.5-1.0	1.0-1.5	1.5-2.0	2.0-3.0	3.0-
CC QE	7%	4%	1%	3%	0%	0%
CC π^0	0%	2%	6%	4%	0%	0%
CC $\pi^{\pm}$	5%	5%	0%	1%	1%	0%
CC $n\pi$	0%	0%	1%	6%	7%	1%
CC others	0%	0%	2%	0%	0%	0%
NC π^0	20%	54%	62%	50%	26%	0%
NC $\pi^{\pm}$	53%	9%	6%	0%	0%	0%
NC $n\pi$	0%	13%	5%	21%	62%	99%
NC others	15%	14%	16%	21%	1%	0%

Acknowledgments

We wish to thank the Super-Kamiokande collaboration, especially the atmospheric neutrino and proton decay group whose efforts produced the world best Monte Carlo event generator and analysis software for water Cherenkov detectors. We also appreciate M. V. Diwan of BNL for fruitful discussions. CY is indebted to P. Paul of Stony Brook University for stimulating discussions and for his careful reading of the draft of this paper. This work was partially supported by the Department of Energy under grant number DEFG0292ER40697

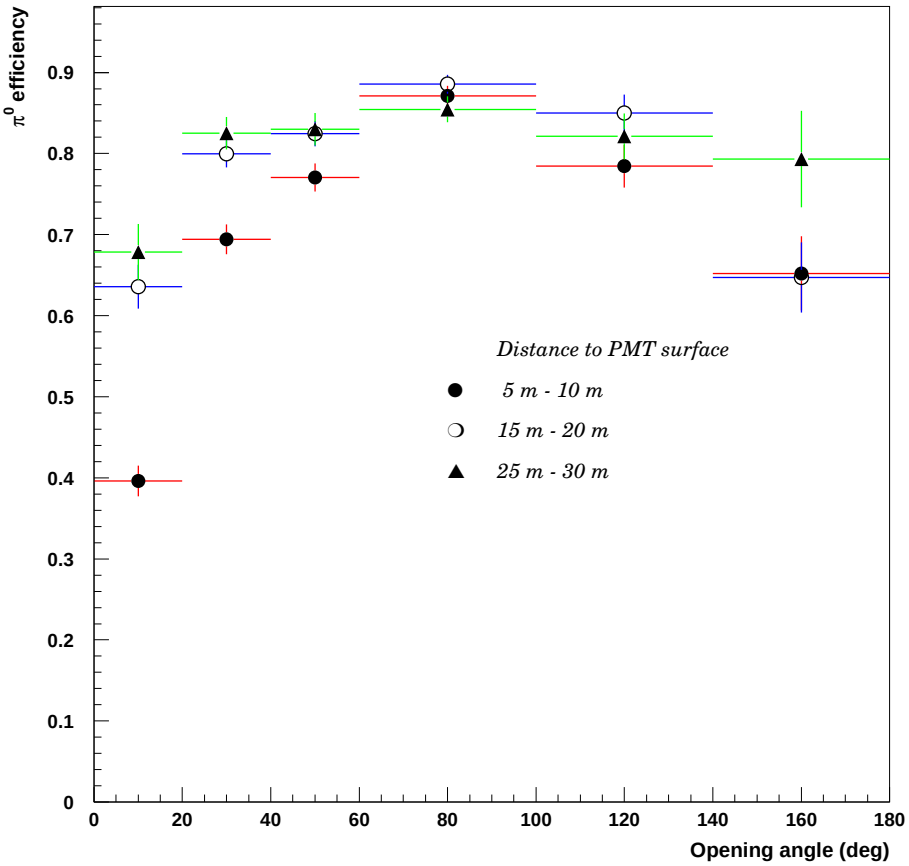

FIG. 29: The π^0 detection efficiency as a function of the two photon opening angle for three ranges of the distance from the π^0 production vertex to the closest PMT surface in the direction of π^0.

(Stony Brook) and DE-AC02-98CH10886(BNL).

---

[1] D. Beavis *et al.*, Report of the BNL neutrino working group, BNL-69395, hep-ex/0211001; M. V. Diwan *et al.*, Phys. Rev. D68, 012002 (2003), hep-ex/0306081.

[2] M. Shiozawa, Nucl. Instr. Meth. A433, 240 (1999).

[3] Y. Ashie *et al.*, Phys. Rev. D71, 112005 (2005).

[4] T. Barszczek, Ph.D Thesis, University of California, Irvine, unpublished (2005). Available at the Super-Kamiokande website at http://www-sk.icrr.u-tokyo.ac.jp/sk/pub/index.html.

[5] Y. Itow *et al.*, The JHF-Kamioka neutrino project, KEK report 2001-4, ICRR-report-

477-2001-7, TRI-PP-01-05, hep-ex/0106019 (2001); C. Yanagisawa, Talk at NNN05, Aussois, France, 2005, available at http://nnn05.in2p3.fr/schedule.html; C. Yanagisawa, Talk at Workshop on Long Baseline Neutrino Experiments, Fermilab, March 6-7, 2006, http://www.fnal.gov/directorate/DirReviews/Neutrino_Wrkshp.html.